ELSEVIER

Enabling 3D printability and vascular morphogenesis with double network dynamic hydrogels

Runze Xu [a], Bohan Dou [a], Shuang Yu [a], Ziyu Wang [c], Yanli Zhang [e], Ling Leng [d], Liliang Ouyang [a,b,*], Wei Sun [a]

[a] Biomanufacturing and Rapid Forming Technology Key Laboratory of Beijing, Biomanufacturing and Engineering Living Systems Innovation International Talents Base (111 Base), Department of Mechanical Engineering, Tsinghua University, Beijing 100084 China
[b] State Key Laboratory of Tribology in Advanced Equipment, Tsinghua University, Beijing 100084 China
[c] Department of Orthopedics, Peking University Third Hospital, Beijing 100191 China
[d] Stem Cell and Regenerative Medicine Lab, Department of Medical Science Research Center, State Key Laboratory for Complex, Severe, and Rare Diseases, Center for Translational Medicine, Peking Union Medical College Hospital, Chinese Academy of Medical Sciences and Peking Union Medical College, Beijing 100730 China
[e] Imaging Core Facility, Technology Center for Protein Science, Tsinghua University, Beijing 100084 China

Hydrogels are crucial biomaterial candidates for tissue engineering and biofabrication applications. The matrix dynamics of hydrogels have recently been demonstrated to contribute to vascular morphogenesis, which is significant for tissue vascularization. However, such dynamic hydrogels are usually mechanically non-stable during culture due to bonding dissociation and cell-mediated degradation, which hinder their usage in advanced biofabricaiton technologies, such as 3D bioprinting. Here, we introduce a double-network dynamic hydrogel (DNDH) bioink strategy to integrate the structural printability, stability, and induction of vascular morphogenesis. Specifically, we synthesize a gelatin-based bioink that is composed of a hydrazone crosslinked dynamic hydrogel network and a methacrylate crosslinked non-dynamic hydrogel network. We demonstrate that our optimized DNDH formulation can be 3D printed into customized structures while retaining structural stability for weeks. Moreover, the DNDH exhibits matrix dynamics with a much shorter stress relaxation time than the non-dynamic counterpart, which is demonstrated to trigger vascular morphogenesis through cell-matrix interactions in a stiffness-independent way. The inclusion of biochemical cues in the matrix and co-culture with supporting cells further enhances the formation of vascular networks and confirms the advantages of DNDH over its non-dynamic counterpart. The *in vivo* studies further confirm the importance of matrix dynamics in vascularization promotion. Our work provides a generalizable and easy-to-use approach to introduce matrix dynamics to bioinks, which could expand the capability of dynamic hydrogels in biofabrication scenarios.

Keywords: Dynamic hydrogel; Double-network hydrogel; Vascular morphogenesis; 3D bioprinting; Bioink

Introduction

Three-dimensional (3D) bioprinting is an advanced biofabrication technology for the engineering of 3D biomimetic tissues at a clinic-relevant scale leading to various downstream applications [1]. Despite current progress, significant challenges to the

* Corresponding author at: Biomanufacturing and Rapid Forming Technology Key Laboratory of Beijing, Biomanufacturing and Engineering Living Systems Innovation International Talents Base (111Base), Department of Mechanical Engineering, Tsinghua University, Beijing 100084, China.
E-mail address: Ouyang, L. (ouy@tsinghua.edu.cn)

https://doi.org/10.1016/j.mattod.2025.01.019

functionality of bioprinted products remain. One major challenge is the lack of capillaries which play an important role in maintaining the physiological functions of native tissues by delivering sufficient oxygen and nutrients, waste removal, as well as coordinating cellular cross-talk [2]. It is highly desirable to replicate a rich microvasculature network in 3D bioprinted tissues *in vitro* to mimic the normal functions of native tissues that are abundant with blood capillaries.

The formation of blood capillaries *in vitro* usually relies on sequential vascular morphogenetic processes of endothelial cells [3,4], including cell adhesion, spreading, migration, and eventual self-organization into capillary-like vascular networks. Previous studies have shown that these cellular processes are triggered not only by biochemical cues, such as the growth factors VEGF, FGF, EGF, etc. [5], but also by physical cues in the 3D microenvironment, such as matrix topology, stiffness, and viscoelasticity [6]. Hydrogels are widely used to mimic the extracellular matrix (ECM) microenvironment and are a major cell carrier in formulating bioinks for 3D bioprinting [7]. Natural protein-derived hydrogels, such as fibrinogen [8] and collagen [9], are frequently used to support morphogenetic processes of vascular endothelial cells under 3D culture conditions. However, the difficulties of bioprinting these hydrogels limit their use as robust bioink candidates. Some semi-synthetic hydrogels such as methacrylated gelatin (GelMA) [10] or norbornene-modified gelatin (GelNB) [11], are used to formulate bioinks because their printability could be readily adjusted via temperature control due to their thermo-responsiveness, while photo-crosslinking induces hydrogel network formation to support a stable 3D culture after printing [12]. Despite the good printability, shape fidelity, and stability under long-term 3D culture, such covalently crosslinked hydrogels might not be easily degraded or remodeled by embedded endothelial cells, thus delaying or hampering the formation of the vascular network [13].

Dynamic hydrogels are reversibly crosslinked hydrogels that have comparable stress relaxation behaviors to native viscoelastic tissues [14–16]. Compared to statically crosslinked gelatin hydrogels (e.g., GelMA, GelNB), dynamic gelatin hydrogels crosslinked via reversible hydrazone bonds significantly enhance matrix-cell interactions to trigger integrin clustering and focal adhesion kinase (FAK) activation of endothelial cells, which further enhance endothelial cell spreading and sprouting into vascular networks [13]. However, dynamically crosslinked hydrogels can be easily dissociated in physiological conditions, which results in the lack of stability to support long-term 3D cell culture. Although solely increasing the crosslinking density improves hydrogel stability, hydrogel dynamics reflected by the stress relaxation property could be consequently diminished. In addition, it is challenging to fine-print dynamic bioinks that are already in a stable gel state, as evidenced by a few recent examples that attempt to translate dynamic hydrogel into dynamic bioinks for extrusion-based 3D bioprinting [17]. Double network strategy [18–21] has been used to formulate double network dynamic hydrogels, which introduce irreversible covalent crosslinks to improve hydrogel stability, while retaining the matrix dynamics that could trigger cellular behaviors. Such hydrogels have been successfully developed as a 3D cell culture platform for cultivating MSCs [22], growth of intestinal epithelial organoids [23], and maintaining the less-inflamed and immature phenotype of monocytes [24], but yet to be investigated in the 3D bioprinting of vascularized tissue constructs.

In this research, we developed a gelatin-based double network dynamic hydrogel (DNDH) system that is composed of both statically crosslinked and reversibly crosslinked hydrogel networks (Fig. 1). Gelatin is selected as the polymer backbones of the DNDH because it provides native cell adhesive motifs, and allows for sufficient cellular remodeling through degradation by the encapsulated cells [25]. We hypothesize that the dynamic domain in the DNDH formulation could promote vascular morphogenesis by stimulating the cell contraction-mediated interactions between endothelial cells and the hydrogel networks, while the non-dynamic component contributes to the printability and 3D culture stability, leading to the 3D bioprinting of tissue constructs with capillary-scale vascularization (Fig. 1). To achieve this goal, we first modified gelatin with methacrylate and hydrazide groups separately to synthesize precursors of the static hydrogel networks GelMA, and the dynamic hydrogel networks GelADH (hydrazide-modified gelatin), respectively. We also synthesized oxidated dextran (DexCHO) as the crosslinker of the GelADH. To obtain the suitable formulation of the DNDH system, we first selected a concentration of the GelMA to serve as the hydrogel base, and then screened the GelADH and the DexCHO concentrations according to the cellular morphology, structural stability and printability. The optimized DNDH formulation was further tested with varying the co-cultured endothelial-fibroblasts cell ratio and supplementation of biochemical cues to further enhance vascular network formation. Under the tested conditions, the DNDH bioink universally outperforms the non-dynamic counterpart regarding vascular morphogenesis in a stiffness-independent manner. We further confirmed this difference by using iPSC-derived endothelial cells, a cell source which is believed to be more therapy-relevant. The demonstration of 3D bioprinting a centimeter-scale structure with built-in microvasculatures, together with the abovementioned evidences suggest that our DNDH formulation could potentially used as a generalizable bioink to engineer vascularized tissues.

Results and discussion

Synthesis and characterization of DNDH components

We obtained the GelMA by directly reacting methacrylate anhydride with gelatin, and obtained the GelADH by modification with adipic dihydrazide via EDC/HOBt coupling reagents. We synthesized DexCHO via sodium periodate oxidation, and used it as the crosslinker of the GelADH to enable the formation of the dynamic hydrogel networks. ^{1}H NMR spectrums show successful modifications of gelatin into GelMA and GelADH respectively (Fig. 2**A**), and modification of dextran into DexCHO (Fig. 2**B**). The proposed crosslinking mechanisms of the interpenetrated double network hydrogel system are predominantly composed of static photo-polymerizable crosslinks among methacrylate groups and reversible dynamic hydrazone bonds among the hydrazide groups on the GelADH and the aldehyde groups on the DexCHO (Fig. 2**C**). We used a TNBS assay [26] to

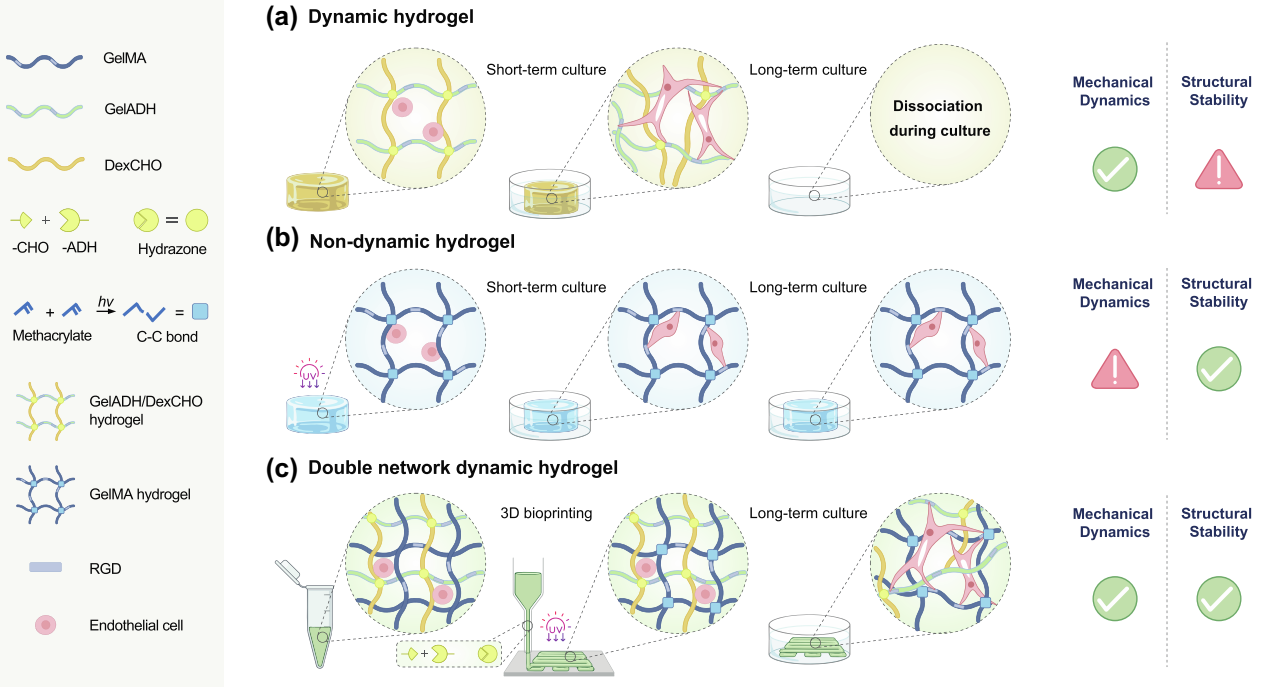

FIG. 1

Schematic illustration of the double-network dynamic hydrogel designed in this study. (A) Dynamic hydrogels provide mechanical dynamics to endothelial cells and regulate vascular morphogenesis. However, such hydrogels are structurally unstable and usually fail to support long-term 3D culture. (B) Typical non-dynamic hydrogels are the major bioink candidates due to their good printability and stability but lack matrix dynamics. (C) The proposed double-network dynamic gelatin hydrogel combines a reversible hydrazone crosslinked dynamic network and a free-radical induced methacrylate crosslinked non-dynamic network. We hypothesize that this combination could retain cell-matrix dynamics for vascular morphogenesis and allow for 3D biofabrication that relies on long-term hydrogel stability, printability and shape fidelity.

quantify the modification degree by detecting the primary amine content on the gelatin backbone (**Fig. S1A**). Using unmodified gelatin and a leucine standard curve as references, the modification degrees of GelMA and GelADH are calculated as 52.0 % and 29.6 %, respectively (**Fig. S1B**). Similarly, by reacting the DexCHO with t-BC and then with the TNBS assay [27], we determined the modification degree of the DexCHO to be 19.4 % (**Fig. S1C**).

Under a physiological pH of 7.4 at room temperature, 5 wt% solutions of Gelatin, GelMA, and GelADH all present as liquid-like with shear moduli lower than 0.1 Pa (Fig. 2**D, E, F**). The inclusion of 1 wt% DexCHO to gelatin or GelMA did not lead to gel formation and contributed little, if not nothing, to the increase of shear modulus (Fig. 2**D, E**). However, an immediate increase of shear moduli was seen by mixing GelADH with DexCHO at a final concentration of 5 wt% and 1 wt%, respectively. The storage modulus (G') rapidly surpassed the loss modulus (G'') and reached ~70 Pa and ~420 Pa at the post-mixing time points of 2 min and 20 min, respectively, leading to a properly self-standing hydrogel (Fig. 2**F**). These results indicate that the possible imine bonds formed between the primary amines of gelatin-based derivatives and aldehyde groups are negligible in the hydrogel network formation, probably due to the overly dynamic kinetics of imine bonds. Thus, the reversible crosslinks that form the GelADH-DexCHO hydrogel are mainly resulted from the hydrazone bonds between the hydrazide and the aldehyde groups. To illustrate the effects of crosslinker density on hydrogel formation, we further included three different concentrations of DexCHO, 0.25 wt%, 0.33 wt%, and 0.5 wt% (equivalent to mass ratio of 1:20, 1:15 and 1:10 to GelADH, respectively), to crosslink the 5 wt% GelADH at room temperature (Fig. 2**G**). All three formulations led to the formation of soft hydrogels with G' less than 100 Pa during 20-minute time-sweep tests. Higher concentration of DexCHO induced faster crosslinking and higher shear moduli; the G' at the 20-minute time point were 17.9 ± 2.7 Pa, 35.4 ± 4.5 Pa, and 78.7 ± 4.5 Pa corresponding to 0.25 wt%, 0.3 wt%, and 0.5 wt% DexCHO groups, respectively (Fig. 2**H**). To demonstrate the mechanical dynamics of the GelADH hydrogels, we carried out stress relaxation test which measures the stress resulted from a constant strain applied to the hydrogels, that corresponds to the resistance to deformation [28]. Compared to 5 wt% GelMA, 5 wt% GelADH crosslinked with various concentrations of DexCHO exhibited a much faster decrease in shear modulus, suggesting a more significant stress relaxation of hydrazone bonds than C–C bonds (Fig. 2**I**). Moreover, lower DexCHO concentration seemed to induce faster stress relaxation. Specifically, the stress relaxation half-time of GelADH hydrogels crosslinked by 0.25 wt%, 0.33 wt%, and 0.5 wt% DexCHO is 1394 ± 275 s, 2348 ± 578 s, and 7289 ± 775 s, respectively, much lower than that ($2.48 \times 10^5 \pm 4.07 \times 10^4$ s) of photo-crosslinked GelMA hydrogel at the same polymer concentration (5 wt%) (Fig. 2**J**).

In order to improve the stability of the GelADH-DexCHO dynamic hydrogels, we sought to add the photo-crosslinkable

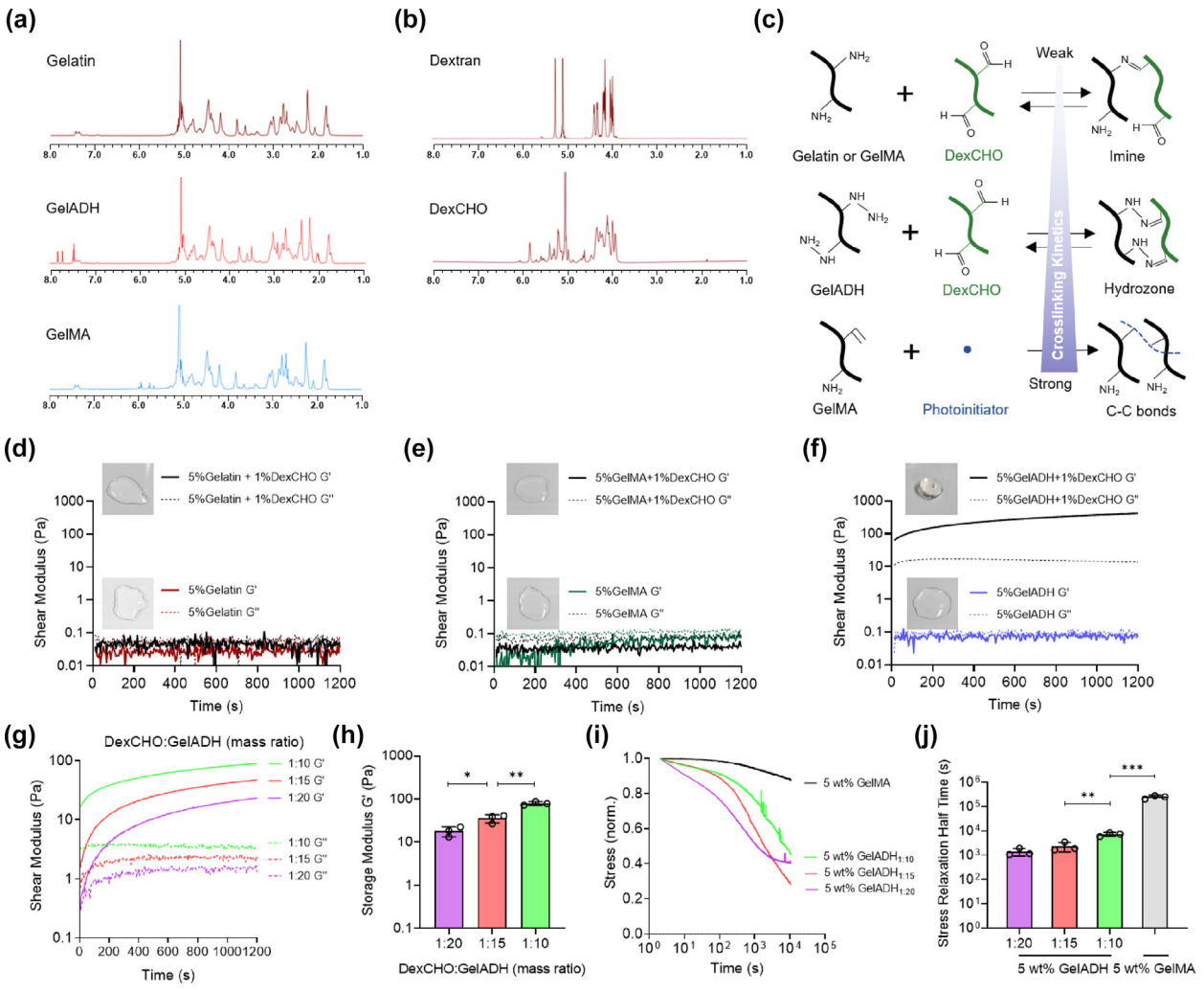

FIG. 2

Synthesis and characterization of double network dynamic hydrogel components. (A) ^{1}H NMR spectrum of gelatin and its derivatives modified with methacrylate and hydrazide, which lead to GelMA and GelADH, respectively. (B) ^{1}H NMR spectrum of dextran and ist derivative modified with $NaIO_4$ oxidation, leading to DexCHO. (C) Three crosslinking mechanisms with different reaction kinetics that occurr in the DNDH system. Rheological time-sweep tests of formulations via mixing crosslinker DexCHO with (D) unmodified gelatin, (E) GelMA, and (F) GelADH. The insert photos represent the optical appearance of hydrogels cast from a cylinder mold using the indicated formulations at 1200 s. (G) Rheological time-sweep test of 5 wt% GelADH dynamic hydrogels crosslinked with different concentrations of DexCHO, and (H) the quantification of storage modulus (G') at 1200 s posting mixing (n = 3). (I) Normalized stress relaxation modulus of 5 wt% GelADH dynamic hydrogels crosslinked with different concentrations of DexCHO, and (J) the quantification of stress relaxation half time (n = 3). Statistical significance is indicated by: *p $\leq$ 0.05, **p $\leq$ 0.01, and ***p $\leq$ 0.001.

GelMA network as enforcement. We screened the concentration of the GelMA hydrogel ranging from 1 wt% to 5 wt% via crosslinking with 405 nm blue light exposure in the presence of 0.1 wt% lithium phenyl-2,4,6-trimethylbenzoylphosphinate (LAP) as photo-initiator. The GelMA hydrogel with a concentration higher than 5 wt% has been demonstrated to hinder the spreading of endothelial cells [13], and thus was not considered in this study. By observing the photo-crosslinked GelMA extruded out from truncated syringe molds from the forward and the front views (**Fig. S2A**), we concluded that 1 wt% GelMA did not form hydrogel, which was further confirmed by time sweeps of photo-rheology tests (**Fig. S2B, S2C**). 2 wt% GelMA showed higher G' (24.7 ± 1.1 Pa) but did not reach a gel strength for self-standing hydrogel formation. 3 wt% GelMA could lead to a standing hydrogel with the bottom part collapsed. In comparison, both 4 wt% GelMA and 5 wt% GelMA formed hydrogel with high shape fidelity, with G' of (360.8 ± 6.4 Pa) and (1090. 2 ± 46.2 Pa), respectively. These data are in good accordance with existing studies [29] that have used GelMA with a similar degree of modification. To further optimize the GelMA concentration, we encapsulated HUVECs (**Fig. S3A**) into GelMA hydrogels in a single cell format and cultured them for 3 days (**Fig. S3B**). We observed that the HUVECs displayed improved spreading morphology on day 3 compared to rounded morphology on day 1 (**Fig. S4**). However, some HUVECs formed cell aggregates in the 3 wt% GelMA, potentially due to local degradation of the GelMA hydrogel by the HUVEC cells and the lack of cell-matrix interactions, in which the adhesions among HUVECs outcom-

pete cell-hydrogel interactions to form cell aggregates. At a GelMA concentration of 4 wt%, HUVECs showed moderate spreading. Further increased the GelMA concentration to 5 wt % resulted in diminished HUVECs spreading, in accordance with previous studies that observed enhanced cell spreading in a softer hydrogel matrix [30].

Here, we selected 4 wt% GelMA as a non-dynamic base hydrogel network to provide hydrogel stability and support the spread of HUVECs. Based on the selected concentration of the GelMA, we also tested the same concentration of the GelADH to investigate whether varying the dynamic crosslinking density of the GelADH-DexCHO dynamic hydrogel could result in differences in HUVECs cell morphology (**Fig. S5**). We found that when the 4 wt% GelADH is crosslinked by a low concentration of DexCHO at 0.2 wt%, the dynamic hydrogel degrades within 24 h, with all the encapsulated cells sedimenting at the bottom of the culture chamber. With a moderate concentration of 0.4 wt % DexCHO, the HUVECs displayed sufficient cell spreading and tended to form connected networks by day 3. At a higher concentration of 0.8 wt% DexCHO, HUVECs spreading on day 3 is diminished. This result is in accordance with a previous study finding that increasing the crosslinker concentration results in an increased crosslinking density of the dynamic hydrogel, which could disrupt the hydrogel matrix dynamics and hence reduce the level of endothelial cell spreading [13].

Optimization of DNDH formulations for 3D printability

We then tested whether the addition of 4 wt% GelMA into the GelADH-DexCHO would improve the shape fidelity and stability of dynamic hydrogel. Throughout the GelADH-DexCHO concentrations to be screened, we set up an orthogonal concentration configuration by selecting the GelADH concentrations ranging from 2 wt% – 4 wt% and three mass ratios of DexCHO to GelADH (1:10, 1:15, 1:20) (Fig. 3**A**). For better communication, we use DNDH-4–$2_{1:20}$ to represent a double network dynamic hydrogel composed of 4 wt% GelMA and 2 wt% GelADH with 1:20 ratio of DexCHO to GelADH, while DH-$2_{1:20}$ represents a dynamic hydrogel alone composed of 2 wt% GelADH with 1:20 ratio of DexCHO to GelADH. The highest concentration of the dynamic hydrogel (i.e., DH-$4_{1:10}$) alone could form a partially standing gel (Fig. 3**B**), but the higher crosslinking density diminished HUVECs cell spreading as indicated in previous experiments. Overall, adding 4 wt% GelMA to the GelADH-DexCHO dynamic hydrogels with subsequent photo-crosslinking leads to significantly improved shape fidelity compared to other orthogonal dynamic formulations supplemented with 2 wt% GelMA or free of GelMA. Upon immersion into phosphate buffer saline (PBS) at 37°C, the dynamic hydrogel formulated in the lowest concentrations (i.e., DH-$2_{1:20}$) dissociated immediately (**Fig. S6**), confirming this formulation alone does not provide stability for 3D cell culture. Adding 4 wt% GelMA as the base hydrogel component to DH-$2_{1:20}$ (i.e., the lowest dynamic content) and DH-$4_{1:10}$ (i.e., the highest dynamic content) both resulted in higher initial storage modulus compared to 4 wt% GelMA alone (Fig. 3**C**). The storage moduli of the DNDH and non-dynamic hydrogels experienced a slight decrease over 7 days of incubation at 37 °C, but still retained 69.9 ± 13.4 %, 75.3 ± 19.0 %, and 73.3 ± 9.1 % of the initial moduli for DNDH-4-$2_{1:20}$, DNDH-4–$4_{1:10}$, and 4 % GelMA, respectively. In contrast, the dynamic hydrogels experienced a dramatic decrease in mechanical properties, the DH-$2_{1:20}$ group could not maintain a proper gel structure and was dispersed readily after being immersed in PBS; the DH-$4_{1:10}$ group with increased dynamic hydrogel concentration could maintain a gel, however, its storage modulus dramatically decreased over incubation time, which dropped to 22.0 ± 11.5 % of its initial storage modulus on day 7 (Fig. 3**C & Fig. S6**). In addition, we labeled the GelADH with fluorescein (FITC) to determine the remaining content of the dynamic hydrogel component in the DNDHs to better understand the stability over time. The results indicated a rapid dissociation of the dynamic network alone – full dissociation for the DH-$2_{1:20}$ group, and only 23.7 ± 2.7 % GelADH was retained on day 7 for the DH-$4_{1:10}$ group (**Fig. S7**). In contrast, DNDH-4-$2_{1:20}$ and DNDH-4-$4_{1:10}$ can retain 65.8 ± 1.3 % and 74.1 ± 4.2 % dynamic components on day 7, respectively. Collectively, these results demonstrated the enhancement of dynamic network stability by incorporating with non-dynamic GelMA network. We further assessed the typical self-healing properties of dynamic networks by placing two hydrogel trunks together at 37 °C for 15 min. Both the DH-$4_{1:10}$ and DNDH-4-$4_{1:10}$ showed considerable adhesion, suggesting that the addition of the photo-crosslinked GelMA network did not interfere with the reversible crosslinking of the dynamic hydrogel networks (Fig. 3**D**).

We also tested the printability of the double network dynamic hydrogel formulations (Fig. 3**E**). The DNDH inks under the orthogonal configurations of dynamic components were printed out and photo-crosslinked, and printability was assessed using previous methods [31]. Two additional groups with an addition of 5 wt% GelMA and with no GelMA were also included. A printability (*Pr*) score that is close to 1 represents the grid structure is well printed with high shape fidelity of the printed hydrogel filament, while low scores indicate poor gelation and high scores indicate over gelation (Fig. 3**F**). We found that the DNDHs with 2 wt% or 3 wt% GelADH and DexCHO to GelADH ratio of 1:15 or 1:20 show acceptable printability, with the *Pr* score ranging from 0.97 to 1.04. To demonstrate the advantages of rapid establishment of large-scale hydrogel scaffold at centimetre-scale, we chose the DNDH-4-$3_{1:20}$ to print out a 10 × 10 mm hydrogel grid scaffold with 5 layers (Fig. 3**G**). The porous square-grid structure contained uniform lattices which allowed for efficient nutrient exchange and could be used as a standardized 3D bioprinting model. To further demonstrate the applicability of the DNDH bioink system to other printing techniques, we seek to print a trifurcated tubular construct in a Carbopol suspension bath (Fig. 3**H**). After printing and photo-crosslinking, the trifurcated tube was transferred into warm PBS at 37°C, the trifurcated structure was well maintained and could self-stand in the air, indicating the good printability and integrity of DNDH bioinks.

The DNDH triggers the spreading and self-assembling of HUVECs towards vascular morphogenesis

We then performed 3D cell culture screening tests over 7 days to select the DNDH formulations that support HUVEC spreading (Fig. 4**A**). Based on previous experiments, 4 wt% GelMA was selected as a base component. The metabolic activity of encapsu-

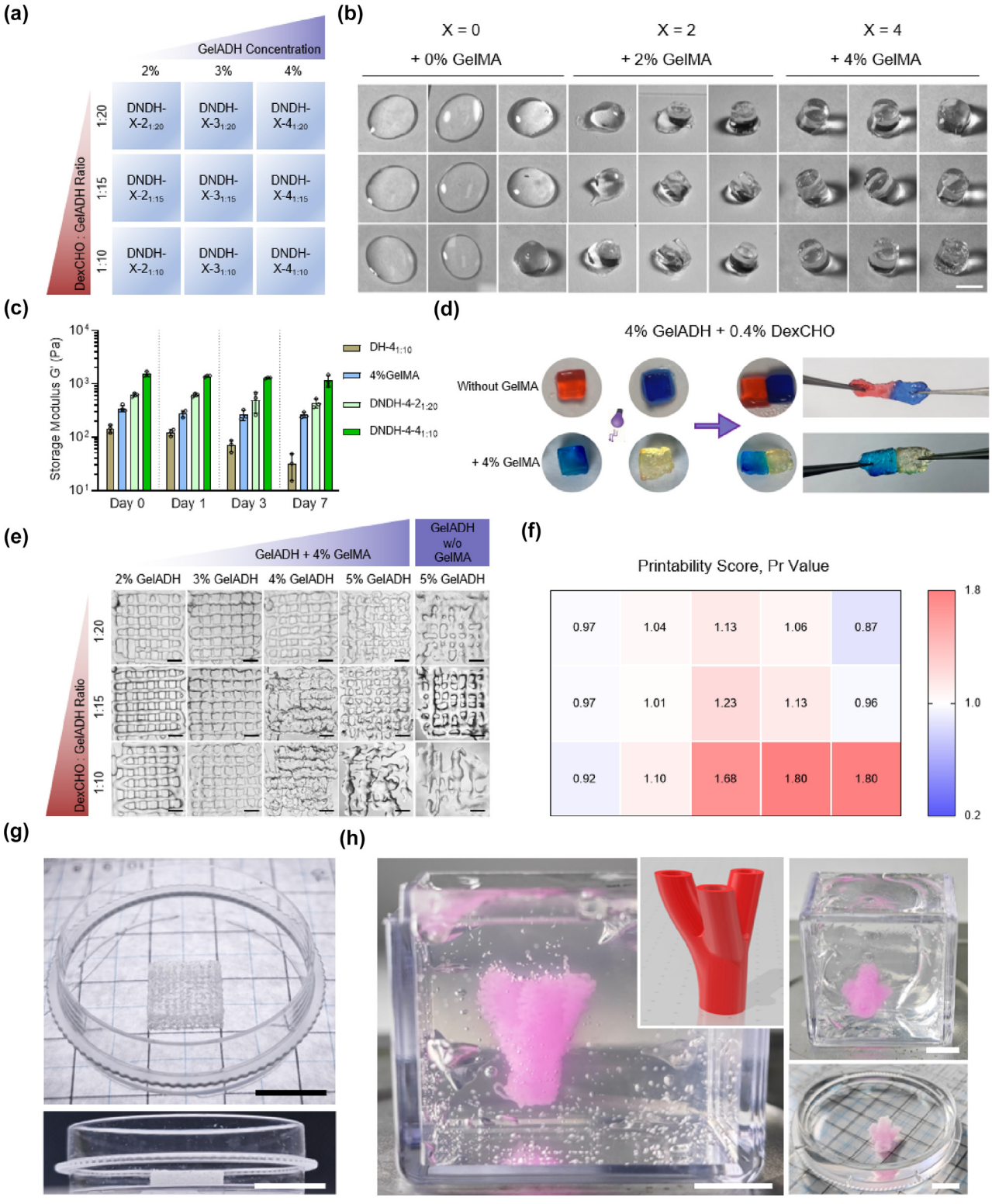

FIG. 3

Optimization of DNDH formulations with material properties suitable for biofabrication process. (A) The orthogonal concentration configurations of the DNDH formulations to be used in this study. (B) Representative photos of cast DNDH cylinder under orthogonal dynamic component configurations and varied concentrations (0–4 wt%) of GelMA, which indicate the differences in shape fidelity post-crosslinking. (C) The storage modulus of hydrogels incubated in PBS at 37 °C over 7 days, showing structural stability in hydrated conditions. (D) After photo-crosslinking, the DNDH pieces exhibited surface adhesion upon putting them together at 37 °C for 15 min. (E) Screening the printability of the DNDH through extrusion bioprinting, and (F) evaluating the printability score of the printed structures. (G) Representative photos of a 3D printed lattice structure (10 × 10 mm, 5 layers) and (H) a trifurcated tubular construct within a suspension bath or PBS after printing. Scale bars: 500 μm (B), 200 μm (E), and 1000 μm (G and H).

lated endothelial cells was assessed through CCK-8 assay, and cells in all the DNDH groups obtained normalized cell metabolic activity of > 95 wt% compared to the 4 wt% GelMA control group (**Fig. S8**). On day 1, HUVECs encapsulated in the groups DNDH-4-$2_{1:20}$ and DNDH-4-$3_{1:20}$ started to show signs of cell spreading, which is different from the rounded cell morphology found in the other groups. On day 3, the level of HUVECs spreading significantly improved for the hydrogel groups with a 1:20 ratio of DexCHO to GelADH. Exclusively, both the groups DNDH-4-$2_{1:20}$ and DNDH-4-$3_{1:20}$ show cell spreading that is greater than the other groups. On day 7, all the hydrogel groups that supported HUVECs spreading on day 3 had decayed cell spreading, potentially because of vascular regression. The group DNDH-4-$3_{1:20}$ seemed to maintain slightly more interconnected cellular networks than the DNDH-4-$2_{1:20}$ group according to the enlarged image of vascular network morphology and quantifying the vascular sprout length (**Fig. S9**). Hence the DNDH-4-$3_{1:20}$ group, short by DNDH*, is selected in the following studies. A zoomed-in view of the HUVECs encapsulated in the DNDH-4-$3_{1:20}$ on day 7 is also shown (Fig. 4**B**). Noticeably, HUVECs in the hydrogel groups crosslinked with a 1:10 ratio of DexCHO to GelADH did not spread well and almost kept their initial rounded cell morphology through the 7-day culture period. This is likely due to the increased crosslinking density of the dynamic

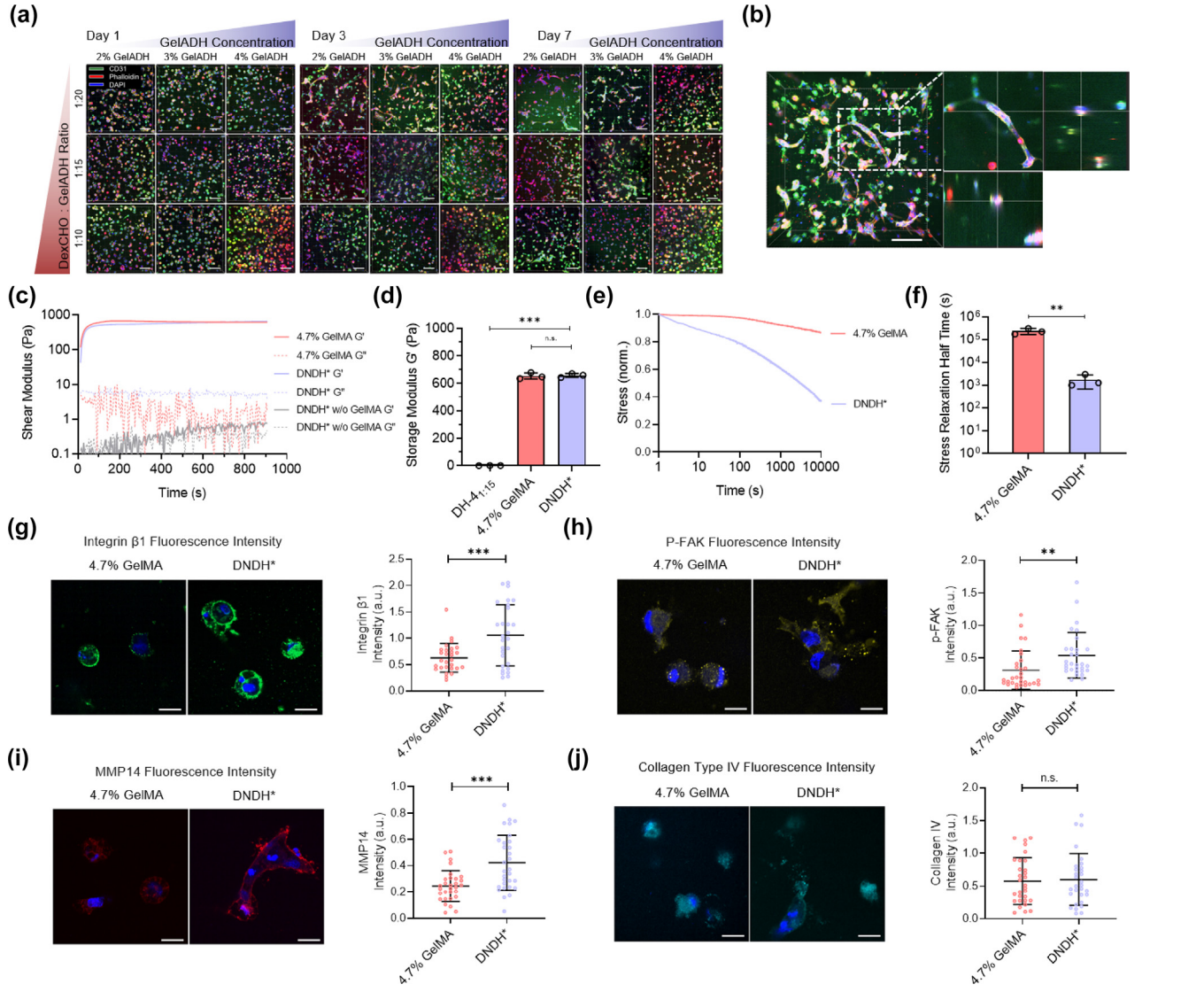

FIG. 4

Comparison of the regulation on HUVECs between DNDH and GelMA with equivalent stiffness. (A) Representative microscope images of HUVECs cultured in the DNDH hydrogels under orthogonal concentration configurations indicate the different cellular morphology during the 7-day culture. (B) An amplified view of HUVECs networks on day 7 in the optimized group DNDH*. (C) Rheological time-sweep tests of 4.7 wt% GelMA and DNDH* formulations in the presence of UV light suggest the gelation process, and (D) the quantified stiffness (n = 3) at plateau phase confirms that the two hydrogel formulations exhibit equivalent stiffness. Light is introduced between 0–180 s under 30 mW/cm^2. (E) The stress relaxation profile and (F) the quantified stress relaxation half-time (n = 3) of 4.7 wt% GelMA and DNDH* hydrogels indicate the difference in mechanical dynamics. The representative fluorescence images and fluorescence intensity quantification of critical mechanotransduction markers (G) integrin β1 and (H) p-FAK at 36 h. The representative fluorescence images and fluorescence intensity quantification of downstream proteins (I) MMP14 and (J) type IV Collagen on day 3. Statistical significance was indicated by: n.s. $p > 0.05$, **$p \leq 0.01$, and ***$p \leq 0.001$. Scale bars, 100 μm (A, B) and 20 μm (G-J).

hydrogel that diminishes the reversible bonding of the hydrogel, resulting in reduced hydrogel dynamics, and eventually constraining the cells to interact with matrix.

We also characterized the material properties of the selected DNDH* through time-sweep rheological testing. With the addition of 4 wt% GelMA and after photo-crosslinking, the G' of dynamic component (DH-$3_{1:20}$) dramatically increased from < 10 Pa to ~660 Pa (Fig. 4**C**), a storage modulus that is sufficient to support hydrogel shape fidelity and stability. To validate the improved cell spreading and cellular network formation, we assessed the expression of markers related to mechanotransduction signaling in the DNDH* through fluorescence quantification. Stiffness is widely believed to be a major mechanical indicator for cell-material interaction studies [32]. To make a fair comparison, we choose a control group of non-dynamic GelMA hydrogel at 4.7 wt%, whose storage modulus after photo-crosslinking is 658 ± 8 Pa, which has nearly the same hydrogel stiffness as that of the dynamic DNDH* group (Fig. 4**D**). The results indicate that the DNDH* group had a stress relaxation half-time of ~2×10^3 s, which is significantly faster than that of 4.7 wt% GelMA (~2.4×10^5 s) (Fig. 4**E, F**). This data clearly shows that the DNDH formulation presents a much more significant stress relaxation behavior than the non-dynamic formulation when the stiffness is held equivalent.

Furthermore, to validate whether the HUVECs embedded in the DNDH* are triggered to spread and subsequently remodel the hydrogel through the relevant molecular signaling pathways, we assessed the expression of integrin and focal-adhesion formation. At 36 h, a time point prior to reaching full cell spreading, the HUVECs encapsulated in the DNDH* group showed enhanced expression of integrin β1 (Fig. 4**G**) and phosphorylated FAK (p-FAK) (Fig. 4**H**), suggesting that the dynamic hydrogel component of the double network hydrogel system has triggered integrin clustering and focal adhesion formation through cell-matrix interactions. This result is in line with a series of studies that utilize dynamic hydrogels to prove enhanced cell spreading of MSCs [22,27,33], myoblasts [14], and HUVECs [13]. Indeed, it is crucial for the cells to first attach to the matrix through integrin binding to cell-adhesive motifs, and then sense the matrix microenvironment by applying cell contraction-mediated traction forces to the matrix [34]. We infer that the matrix dynamics and the native cell-adhesive motifs on the gelatin backbones of the DNDH promoted HUVECs spreading similarly. On day 3, the DNDH* group allowed the HUVECs to degrade the double hydrogel networks with significantly increased matrix metalloproteinase 14 (MMP14) expression (Fig. 4**I**). The deposited content of type IV collagen was also assessed because it is one of the functional components of the vascular basement membrane. Both the DNDH* and the 4.7 wt % GelMA groups deposited similar levels of type IV collagen (Fig. 4**J**), which indicates they both facilitate the HUVECs to remodel the hydrogel matrix. Additionally, to demonstrate the generalization of our DNDH in promoting the growth of more cell types, we cultured human mesenchymal stem cells (MSCs) and hepatocellular carcinoma cell line (HepG2) spheroids as stem cell and cancer cell representatives, respectively, within the DNDH* and 4.7 wt% GelMA. We found that the DNDH triggered a higher degree of MSC spreading, with an increased cell aspect ratio and more spreading morphology (**Fig. S10**). We also observed greater size expansion of the HepG2 spheroids cultured in the DNDH* compared to those in the GelMA group (**Fig. S11**). These data collectively show our DNDH is generalizable to support the spread and growth of more cell types.

To establish stable vascular networks, we sought to co-culture the HUVECs with human lung fibroblasts (HLFBs) to improve vascularization in the optimized DNDH* group. Co-culturing of vascular endothelial cells with MSC, HDFs, and pericytes supports vascular stabilization and maturation for the *in vitro* angiogenesis process taking place in bulk hydrogels [8–10,35]. In our study, HLFB was selected because human lung tissue is highly vascularized, and HLFBs play vital roles in stabilizing capillaries through cell–cell contacts and growth factors secretion [36]. The embedded cell ratios of the endothelial cells to stromal cells could influence vascular morphogenesis. We tested three ratios of HUVECs to HLFBs (4:1, 2:1, 1:1) based on the optimized DNDH* formulation, with a fixed cell density of HUVECs at 4 million cells mL^{-1} (**Fig. S12**). On day 1, altering the HUVECs to HLFBs cell ratio did not influence the cell spreading within the DNDH*, because the cells were still probing and remodeling the hydrogel matrix prior to spread. However, we observed that on day 3, co-cultured HUVECs and HLFBs spread and formed interconnected vascular networks for all the cell ratios. We found that at a ratio of 2:1 for HUVECs to HLFBs, a stable vascular network is formed among HUVECs and HLFBs which could be maintained to day 7. At a lower HUVECs to HLFBs ratio of 4:1, there is a limited number of HLFBs to interact with the HUVECs, resulting in a vascular network that is slightly more interconnected than the mono-cultured HUVECs without HLFBs. Co-culturing at a higher HUVECs to HLFBs ratio of 1:1 led to 3D hydrogel spaces over-dictated by the HLFBs. Therefore, the HUVECs to HLFBs ratio of 2:1 was adopted in the remaining sections of the study to culture vascular networks with improved vascular morphogenesis. In comparison with the literature, HUVECs have been co-cultured with stromal cells to support vascular network formation in other types of hydrogels, in various ratios of 1:2, 1:1, and 3:1, respectively [8–10,35], which might be influenced by the specific types of cells and hydrogels.

To investigate the maintenance of DNDH mechanical strength with the cell remodeling during culture, we assessed the storage modulus of the DNDH* hydrogel co-encapsulated with HUVECs and HLFBs at the 2:1 ratio over 7 days of culturing. The 4.7 wt% GelMA (with equivalent stiffness of the DNDH*) and 4 wt% GelMA (the non-dynamic base component of the DNDH*) were selected as non-dynamic control groups. An overall decrease in stiffness was seen for the individual hydrogel groups. Though exhibiting an equivalent initial stiffness, the hydrogel stiffness of the DNDH* was slightly lower than that of the 4.7 wt% GelMA group at each assessment time point, without significant differences (**Fig. S13**). This is likely due to the enhanced cell-mediated hydrogel degradation for the dynamic networks. Though the DNDH* was weakened during culture, it still retained ~65 % and ~60 % of its initial modulus on day 3 and day 7, respectively. Moreover, the DNDH* had overall higher hydrogel stiffness than the 4 wt% GelMA group over 7-day incubation. To better understand the timeframe of the dynamic component interactions with the cells, we further

characterized the degradation of the dynamic networks by monitoring the GelADH release from the DNDH* at different culturing time points (**Fig. S14**). The GelADH was seen with an obvious release from the DNDH* either in the presence or absence of cells, with most of the dissociation happening in the first 3 days. Nevertheless, there were still considerable dynamic networks remaining; the remaining GelADH was 67.4 ± 1.5 % and 57.6 ± 1.4 % for acellular and cell-laden DNDH* on day 7, respectively. We reasoned the higher amount of GelADH degradation with the cell culturing was because the cells have remodeled the DNDH* to a greater extent by deforming the hydrogel matrix to spread, while also degrade the hydrogel with MMPs.

Coupling biochemical and biological cues improves vascular network formation and confirms the importance of dynamics in DNDH

In addition to triggering *in vitro* vascular morphogenesis using the DNDH's physical cues and the slight amounts of biochemical factors contained in the culture medium that are intended to support endothelial cell expansion, we also tested whether the supplementation of VEGF and laminin could further stimulate vascular network formation. The growth factor VEGF [37] was chosen because it has known effects of triggering angiogenesis. Laminin is one of the vascular basement membrane components and was selected because previous study has shown that laminin maintains vascular integrity [38]. It could be retained in hydrogels due to its large molecular weight [39]. Upon the addition of 50 ng mL^{-1} VEGF to the culture medium and 100 μg mL^{-1} laminin to the hydrogels, vascular network formation was assessed over 7 days of culture with 4.7 wt% GelMA (Fig. 5**A**), 4 wt% GelMA (**Fig. S15**) and DNDH* (Fig. 5**B**). The vascular tube length (Fig. 5**C**) and mean tube volume within every visual region of 0.156 $μm^3$ (Fig. 5**D**) were further quantified based on the confocal fluorescent image stacks. Without additional supplementation, the DNDH* group supports higher vascular tube length and higher mean tube volume in comparison to the 4.7 wt% GelMA. This proves that dynamic hydrogel components are crucial to vascular morphogenesis independent of stiffness. The DNDH* group also resulted in higher vascular tube length compared to the 4 wt% GelMA group bearing the same GelMA concentration but without the dynamic hydrogel component.

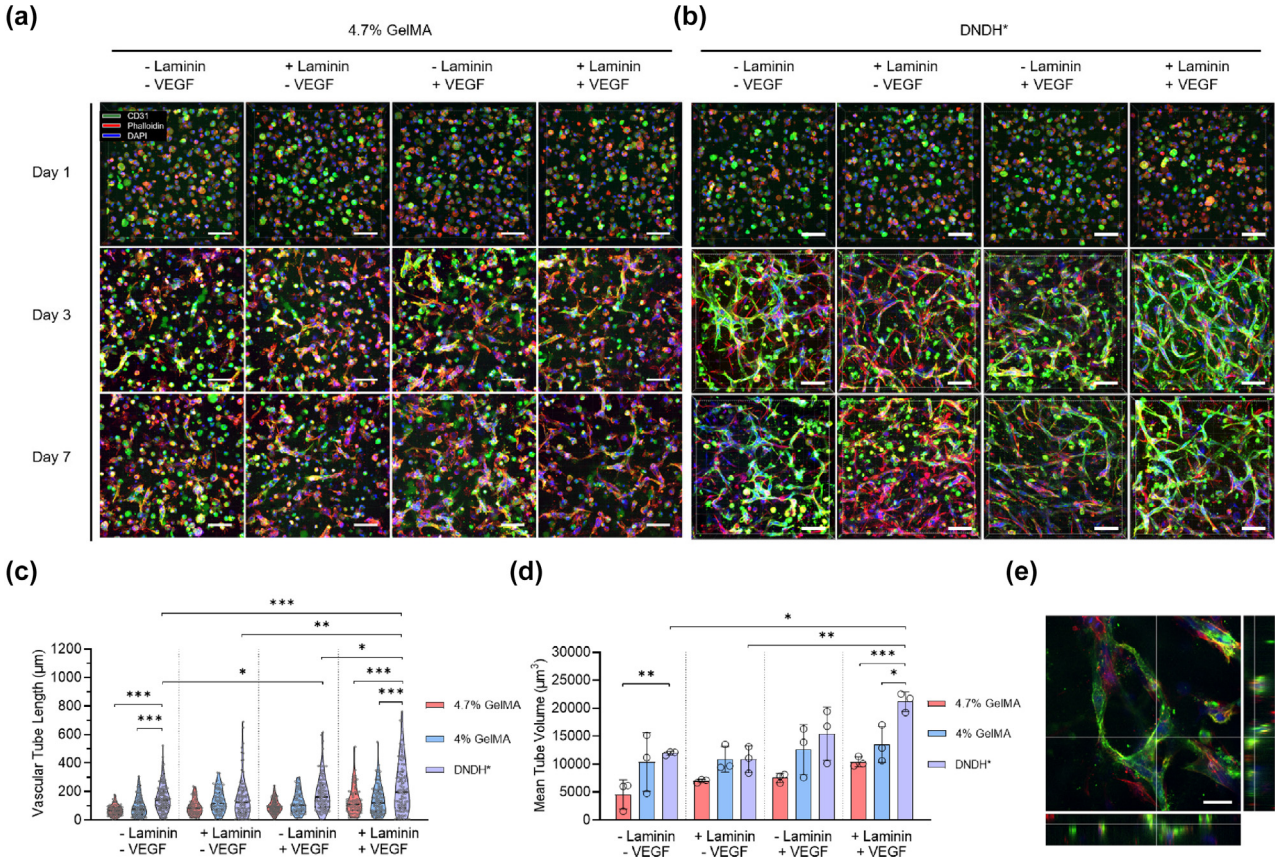

FIG. 5

The inclusion of biological and biochemical cues further enhances the vascularization in the DNDH. (A) Representative confocal images of formed vascular networks in the (A) 4.7 wt% GelMA and (B) DNDH* hydrogels under HUVECs-HLFBs co-culture (cell amount ratio 2:1) in the presence or absence of laminin (100 μg mL^{-1}) and VEGF (50 ng mL^{-1}) for 7 days. Quantification of the co-cultured (C) vascular tube length and (D) mean tube volume in the 4.7 wt% GelMA, 4 wt% GelMA, and the DNDH* groups with different configurations of laminin and VEGF. (E) A representative max intensity projection of the vascular network junction on day 3 in the DNDH* group with the inclusion of laminin and VEGF. Statistical significance was indicated by: *$p \leq 0.05$, **$p \leq 0.01$, and ***$p \leq 0.001$. Scale bars, 100 μm (A-B) and 40 μm (E).

The comparison between the DNDH* group and the 4 wt% GelMA group shows even if the dynamic hydrogel component eventually dissociates and is not retained in the hydrogels, their initial presence has a significant effect in triggering vascular morphogenesis through the provided cell-matrix dynamics. Under the condition of adding both the VEGF and laminin, the DNDH* group led to improved vascular tube length (mean = 228.4 μm) when compared to the 4.7 wt% GelMA (mean = 132.5 μm) and the 4 wt% GelMA group (mean = 140.9 μm), and larger mean tube volume (mean = 21192.6 μm^3) compared to the 4.7 wt% GelMA (mean = 10413.4 μm^3) and the 4 wt% GelMA group (mean = 13528.9 μm^3), suggesting that hydrogel dynamics in combination with biochemical supplementation together facilitate the vascular network formation (Fig. 5**C**). We found that for the DNDH* group, adding VEGF alone slightly increased vascular tube length (mean = 186.4 μm), while supplementing laminin alone to the hydrogel appeared to result in a higher upper limit value of the vascular tube length, although it was not statistically significant. The addition of both the VEGF and laminin further increased the vascular tube length compared to adding VEGF or laminin individually, which suggests that there is a combinatorial effect of laminin and VEGF on the HUVECs. These results are in line with several existing studies that prove laminin's affinity to VEGF, while laminin could also upregulate VEGF uptakes by endothelial cells [40–42]. An enlarged view of the formed vascular networks in the DNDH* group when added with VEGF and Laminin is presented (Fig. 5**E**), with the uniform distribution of the formed vascular networks shown in 3D (Supplementary video 1).

To further demonstrate the clinical potential of the DNDH formulation, we explored whether the DNDH hydrogel could support iPSC-derived endothelial cells (iECs) self-organization. The successful differentiation of vascular endothelial lineage was verified by examining some typical markers, including CD31, VE-Cadherin (VE-Cad), ICAM-1, and vWF (**Fig. S16**). We have also assessed their reorganization function of the iECs using the Matrigel-based *in vitro* tube formation assay (**Fig. S17**), which confirmed the functionality of the iECs. Under optimized co-culture conditions and the addition of VEGF and laminin, both the DNDH* group and the 4.7 wt% GelMA support iECs and HLFBs self-assembly into microvascular networks (**Fig. S18**). In comparison to the 4.7 wt% GelMA group, the DNDH* group led to enhanced vascular tube length on both day 3 (1.27-fold) and day 7 (1.34-fold), while the mean tube volume of the vascular networks was improved on day 7 (1.35-fold). The iPSC-sourced iECs exhibit features of vascular development and mimic vascular pathology [8,43]. Embedding the iECs into hydrogels could give rise to an *in vitro* functional or diseased vascular model, as well as serving as a potential vascularized tissue replacement. Conventionally, iECs could be 3D cultured with hyaluronic acid-based hydrogels [44] or natural protein-derived hydrogels [8,45]. These hydrogels are either statically crosslinked, which hamper vascular network formation, or could not be readily printed as a vascularized bioink due to the narrow bioprinting window. Our DNDH allows for vascular network formation from the iECs while maintaining stability and printability. We envision that our DNDH has the potential to fill the gap in 3D bioprinting iPSC-derived vascularized tissue constructs.

3D bioprinting of DNDH bioink into capillary-scale vascularized tissue mimetic construct

To evaluate whether the DNDH could serve as a versatile bioink for printing large-scale vascularized tissue constructs, we demonstrated the printing of a 4-layer 3D grid structure with a size of 8 × 8 mm using the optimized conditions. We choose to print a representative grid-like standard structure, which allows for sufficient oxygen and nutrient transfer among hydrogel filaments, compared to cells embedded in bulk hydrogel. To assess the structure stability of the printed structure using our optimized DNDH bioink, the diameter of the filament was measured at different time points during culture, which did not change much over time (Fig. 6**A**). We found that the printed cells exhibited considerable cell viability during a 7-day culture (Fig. 6**B**). The increased extent of cell spread and migration resulting from multi-cellular network assembly has given rise to difficulties in identifying the number of living cells through the Live/Dead™ staining images. To alternatively assess cell viability, we performed the CCK-8 assay to evaluate the general metabolic activity of the embedded cells over the culturing period (Fig. 6**C**). Consistently to the reduced viability, we confirmed the general metabolic activity of co-embedded HUVECs and human lung fibroblasts (HLFBs) decreased slightly over the 7 days culture in the DNDH* bioink (Fig. 6**C**). This decay in the general cellular metabolic activity is also confirmed using the alamarBlue™ assay (**Fig. S19**). We reasoned that the metabolic activity decay is due to the remodeling and regression of the vascular networks after their formation. This finding is consistent with a series of previous studies that reported negligible proliferation or even a decreased number of vascular endothelial cells over time when cultured in 3D gelatin-based hydrogel [10] and a synthetic hydrogel [46], and decreased cell metabolic activity of vascular spheroids co-assembled with fibroblasts [47].

Along the post-printing culture period, the HUVECs and HLFBs self-organized into micro-vascular networks within the printed bioink filaments as similarly observed in the 3D cultured condition without printing. A full view of the printed vascularized construct shows the uniform distribution of the cells as well as the morphology of cells within the entire printed constructs (Fig. 6**D**). An enlarged view of the window surrounded by the filament lattice was also presented (Fig. 6**E**). We observed the formation of vascular networks in the printed DNDH* filament lattice, as in the non-printed DNDH* samples, under the same optimized conditions. This proves that the DNDH could serve as a vascularized bioink for extrusion-based rapid 3D bioprinting of tissue mimetic constructs that have a clinical-relevant scale.

The DNDH facilitates in vivo angiogenic effects

To further show the potential of the DNDH in facilitating *in vivo* tissue angiogenesis, We carried out transplantation of the DNDH subcutaneously into Sprague Dawley (SD) rats. In order to investigate the coupled role of combining mechanical cues and biochemical cues, four groups of hydrogels are set to match the *in vitro* work in the previous sections of this study. We compare the DNDH* group to the 4.7 wt% GelMA group with the same hydrogel stiffness, both supplemented with or without VEGF, leading to the groups of 4.7 wt% GelMA, DNDH*, 4.7 wt% GelMA + VEGF, and DNDH* + VEGF. We examine the trans-

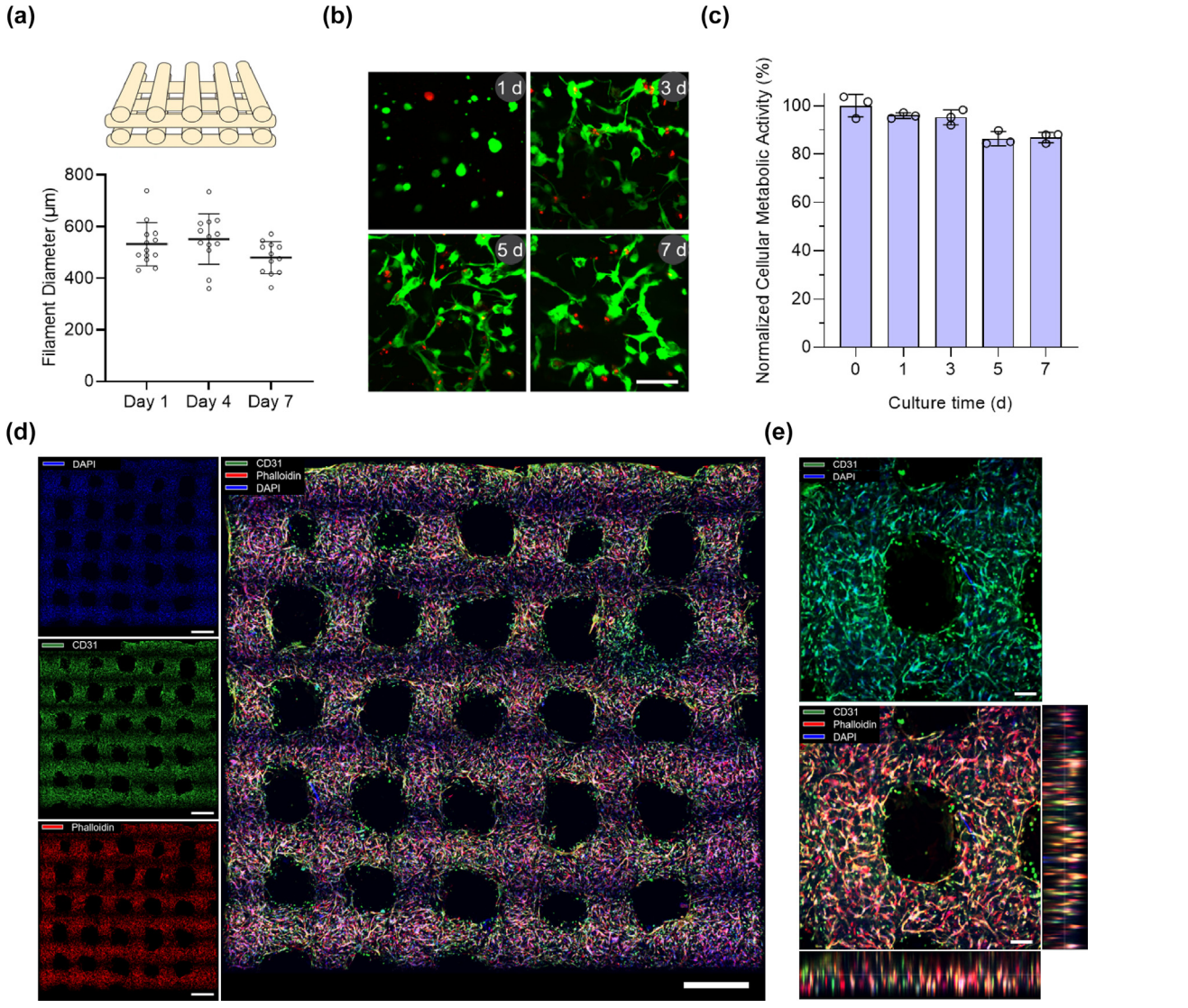

FIG. 6

The DNDH bioink could support the long-term culture of the 3D bioprinted vascular construct. (A) Quantification of the scaffold filament diameters after bioprinting (n = 3). (B) Live/Dead™ staining and (C) normalized cellular metabolic activity (n = 3) of the co-cultured HUVECs and HLFBs embedded in the 3D printed structures during 7-day culture. (D) The full-view and (E) representative enlarged view of a 3D printed vascularized multi-layered lattice construct on day 7. DNDH* formulation and optimized biochemical and biological cues are used for (A-E). Scale bars, 100 μm (C), 1000 μm (D), and 200 μm (E). Statistical significance was indicated by: *$p \leq 0.05$.

planted hydrogel samples by H&E staining, Masson staining, immunofluorescence staining, and observing the infiltration of perfusable capillaries into the hydrogels. The H&E staining reveals that all the groups at 1 week have been infiltrated by peripheral tissue cells as considerable cell nuclies are identified in the hydrogel boundary region, which is a significant sign prior to *in vivo* angiogenesis (Fig. 7**A**, upper). However, the duration of 1 week is not long enough for the tissue-resident cells to migrate into the central part of the hydrogels. This is similar to the *in vivo* angiogenesis during wound healing, during which the inflammation phase occurs first [48]. The majority of the migrated cells at the 1-week stage are likely to be macrophages and fibroblasts, as evidenced by literature [49]. During sample harvesting (Fig. 7**A**, figure insets), we observed the DNDH* groups better integrated into the native tissue compared to the GelMA groups, as the DNDH* groups had more peripheral tissues connected and were less transparent. This is also supported by Masson staining (Fig. 7**A**, lower), which indicates the invaded cells have deposited collagen as a major ECM to remodel the hydrogels. At week 2, we found that all the hydrogel groups had been invaded by cells in the hydrogel center to varied extents (Fig. 7**B**, upper). The 4.7 wt % GelMA group without VEGF showed visually less cell infiltration and permitted limited host capillary invasion than other groups. This suggests the importance of both VEGF and hydrogel matrix dynamics in facilitating wound healing and angiogenesis. The less transparency of the hydrogels at week 2 (Fig. 7**B**, figure insets), together with Masson staining (Fig. 7**B**, lower) indicates that cells from peripheral tissues have tightly surrounded and invaded the hydrogels, leading to more hydrogel remodeling. The groups, except for the 4.7 wt% GelMA, have all been infil-

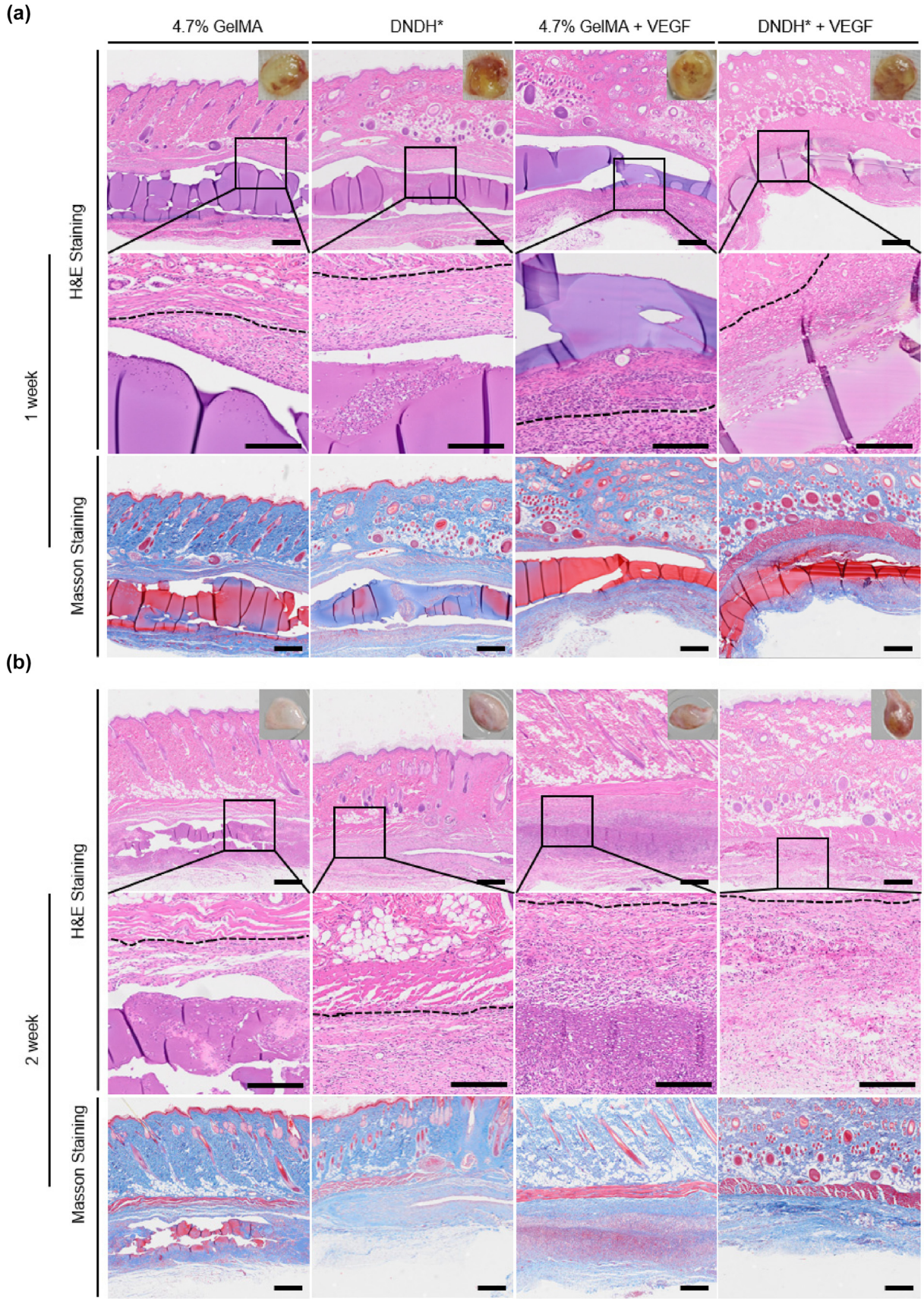

FIG. 7

Cell infiltration from peripheral tissue into hydrogels *in vivo*. Representative H&E staining across the entire subcutaneous region and zoomed-in view (upper), the harvested hydrogel samples (insets), and Masson staining (lower) at (A) week 1 and (B) week 2. Scale bars, 500 μm, 200 μm (zoomed-in images).

trated through their entire hydrogel regions, as evidenced by more replicates **(Fig. S20)**.

To assess whether the functional neovasculatures have formed in the hydrogels, we double stained the hydrogel sections with CD31 and α-smooth muscle actin (αSMA) to identify functional blood vessels. At week 1, we saw neovasculature formation at the hydrogel-tissue interfaces for DNDH*+VEGF group as evidenced by co-localization of CD31 and αSMA (Fig. 8**A**). Though the DAPI shows cellular infiltration towards the hydrogel center from the edge, vascular morphogenesis has not yet been observed in the hydrogel center, in consistent with our histology staining results. At week 2, *in vivo* angiogenesis of the hydrogels has achieved to a greater extent, with all the groups seen with established blood vessels in the implanted hydrogels to varied extents (Fig. 8**B**). We quantified the vascular density by counting the vascular structure with a co-localized expression of CD31 and αSMA per square milimeter (Fig. 8**C**), and vascular sprouting distance from the hydrogel-tissue interfaces (Fig. 8**D**). Compared to the 4.7 wt% GelMA group, the DNDH* group shows higher vascular density at week 1, and higher sprouting distance at both

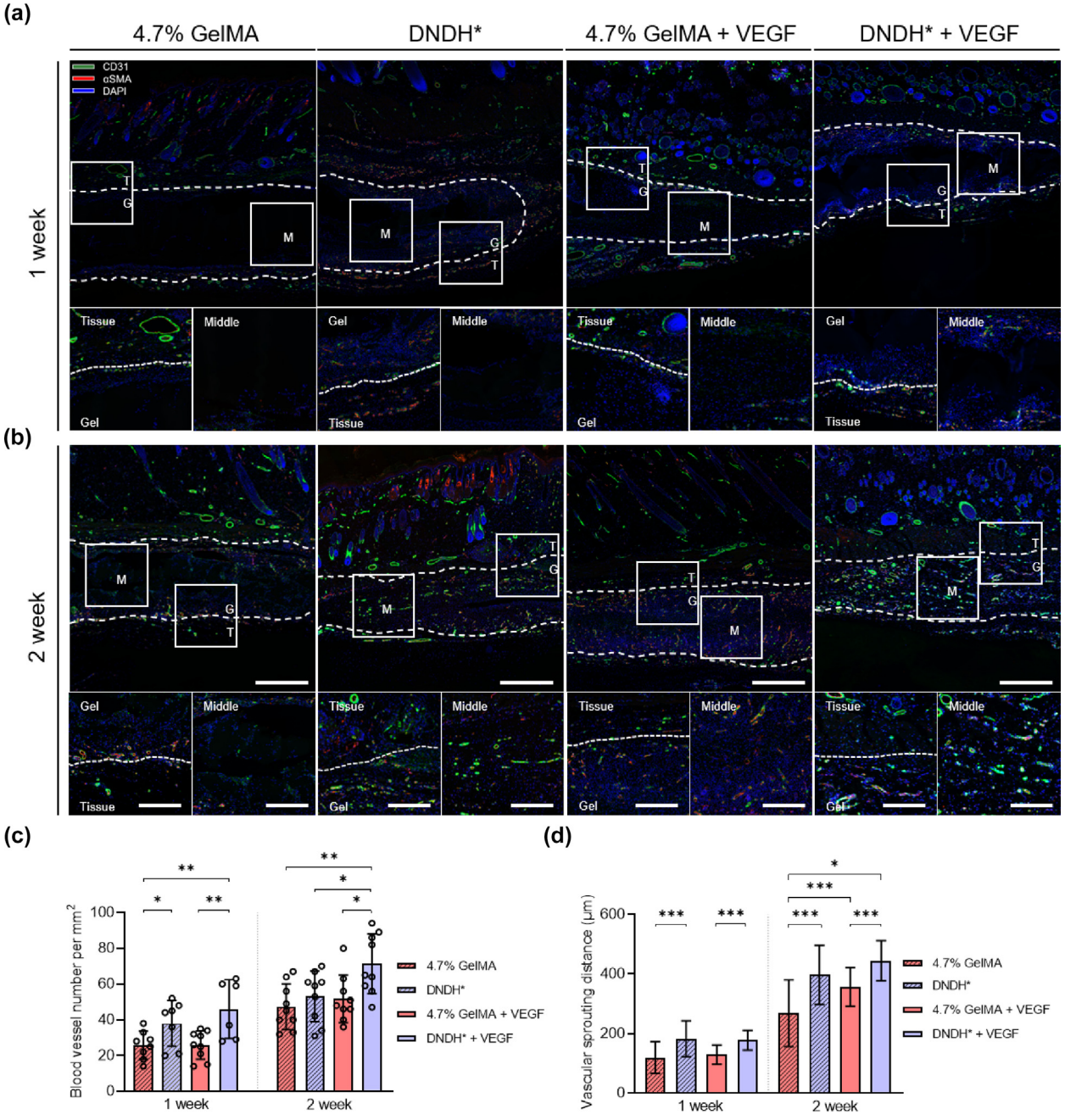

FIG. 8

Validation of *in vivo* angiogenesis process. (A) Immunofluorescent staining with CD31 and α-smooth muscle actin (αSMA) to assess neovasculature in the transplanted hydrogels at 1 week and 2 week. The zoomed-in view at the hydrogel-tissue interfaces and the middle region of the hydrogels are shown in figure insets. (B) Quantification of *in vivo* angiogenesis with vascular density and sprouting distance. Statistical significance was indicated by: *$p \leq 0.05$, **$p \leq 0.01$, and ***$p \leq 0.001$. Scale bars, 500 μm (A), and 200 μm (zoomed-in figure insets).

week 1 and week 2. This indicates that the DNDH could facilitate early *in vivo* angiogenesis in a manner dependent on matrix dynamics. At week 2, the supplementation of VEGF further increases the vascular sprouting distance of the 4.7 wt% GelMA group. The inclusion of VEGF also increases the vascular density of the DNDH* group, compared to the plain DNDH* group. Together, the DNDH* + VEGF group has the highest vascular density and sprouting distance throughout the 2 weeks. These data suggest that the DNDH* facilitated greater angiogenesis *in vivo* compared to the non-dynamic counterpart at a similar stiffness. In addition, matrix dynamics and VEGF supplementation can combinatorially accelerate *in vivo* angiogenesis. We further injected fluorescence-labeled dextran (Dextran-FITC) into the tail vein of the SD rats at week 2 before harvesting and visulizing samples. The harvested hydrogels are later observed to support Dextran-FITC flowing in blood vessels, indicating the established vasculature in the hydrogels is functionally perfusable (**Fig. S21**).

The *in vivo* angiogenesis is a highly complex process that involves orchestrated cellular behaviors of multiple cell types, such as fibroblasts, endothelial cells, and pericytes. The matrix dynamics provided by dynamic hydrogels have been proven to support the spreading of fibroblasts [50], or endothelial cells [13], which are all crucial cell types in angiogenesis process. In this study, we attribute the enhancement of *in vivo* angiogenesis to the invasion of vascular endothelial cells and their supporting cells from the peripheral tissues, which are promoted by matrix dynamics of the DNDH. Compared to other non-degradable dynamic hydrogels used as *in vitro* tools to research cellular behaviors, our gelatin-based DNDH is degradable in response to cellular secreted enzymes, for example, the MMPs, which allows for cell-mediated degradation to sufficiently remodel the hydrogel into native *in vivo* cellular microenvironment. Besides, the extent of matrix dynamics may affect *in vivo* angiogenesis. The over-enhanced cell contractility due to hyper matrix dynamics could down-regulate vascular endothelial cadherin (VE-Cadherin) and disrupt the intercellular adhesions, which led to diminished vascular sprouting and invasion compared to the hydrogels with medium matrix dynamics [51]. The DNDH* used in our study has a stress relaxation half-time of thousands of seconds, which could be considered as dynamic hydrogels without hyper dynamics, that secures the angiogenic effects. Our opinion is supported by studies that concluded supramolecular dynamic hydrogels with excessively dynamic behavior could lower the binding energy of the integrin-matrix complex, and hence hinder the downstream mechanotransduction [52]. Finally, physical and biochemical cues could couple to trigger vascular endothelial cell behaviors, which has been investigated *in vitro*, for example, VEGF receptor activity of HUVECs could be regulated by blood flow-induced shear stress [53]. We anticipate that integrating the matrix dynamics of the DNDH with other types of biochemical cues involved in the wound healing stages would further expand the clinical potential.

Conclusion

Our work highlights the importance of matrix dynamics beyond stiffness for vascular morphogenesis and introduces a double network dynamic hydrogel (DNDH) bioink approach to fill in the gap between structural printability/stability and vascular morphogenesis. The studied DNDH is composed of statically methacrylate crosslinked networks and reversibly hydrazone crosslinked hydrogel networks. Both components are gelatin-based to provide cell adhesion and cell-mediated degradability. Our DNDH system has improved matrix dynamics as characterized by the shorter hydrogel stress relaxation time in comparison to a purely statically methacrylate crosslinked hydrogel at an equivalent stiffness. Utilizing the double network strategy leads to improved hydrogel dynamics while ensuring hydrogel stability. More importantly, our DNDH bioink allows enhanced HUVECs spreading into cellular networks. Using the screened formulation of the DNDH, we optimized the cell ratio of HUVECs co-cultured with HLFBs, and then investigated the effects of adding additional biochemical cues such as VEGF and laminin on vascular network formation. We also show that under the optimized conditions, iPSCs-derived ECs could also form vascular networks. The versatility of our DNDH bioink is illustrated by establishing vascularized constructs via extrusion-based 3D bioprinting and *in vivo* subcutaneous implantation. By demonstration of rapidly established large-scale vascularized constructs, we prove that the DNDH hydrogel could be used as a general vascularization bioink, which is clinically relevant and has broad applications when establishing vascularized tissue constructs through extrusion-based 3D bioprinting.

Experimental section

Cell culture

Human Umbilical Vein Endothelial Cells (HUVECs, CRL-1730, ATCC) were maintained in endothelial growth medium (EGM2, Lonza) with medium change every 2 days, and were passaged with Accutase cell detachment solution. Human Lung Fibroblasts (HLFBs, kindly provided by Dr. Tiankun Liu) were maintained in BASIC MEMα (Gibco) supplemented with 10 v% fetal bovine serum (VivaCell), 50 μg mL^{-1} ascorbic acid (Sigma–Aldrich), 5 μg mL^{-1} recombinant human insulin (Sigma–Aldrich), and 5 ng mL^{-1} recombinant human bFGF (Peprotech), with medium change in every 2 days and were passaged with 0.05 wt% Trypsin-EDTA (ThermoFisher Scientific). Human Mesenchymal Stem Cells (MSCs, human umbilical cord) were maintained in MesenCult™ (STEMCELL Technologies) with medium change every 2 days and were passaged with 0.05 wt% Trypsin-EDTA (ThermoFisher Scientific). Hepatocellular Carcinoma Cell Line (HepG2) were maintained in Eagle's Minimum Essential Medium (EMEM, ThermoFisher Scientific) supplemented with 10 v% fetal bovine serum (VivaCell), with medium change every 2 days, and were passaged with 0.05 wt% Trypsin-EDTA (ThermoFisher Scientific). The HepG2 spheroids were obtained by seeding single HepG2 cells into 24-well AggreWell™400 microwell culture plates (STEMCELL Technologies), at a cell density of 1×10^6 cells mL^{-1} and culturing for 2 days.

hiPSC maintainance and vascular endothelial cell differentiation

Human iPSCs were provided by the Stem Cell and Regenerative Medicine Lab of Peking Union Medical College Hospital. hiPSCs

were maintained on Matrigel (Corning) coated 6-well plate (Corning) in mTeSR1 medium (STEMCELL Technologies). For differentiating hiPSCs into vascular endothelial cells, hiPSCs were digested into single cells with Accutase (STEMCELL Technologies) and seeded on Matrigel-coated 6-well plates at a density of 5000 to 10,000 cells/cm^2 in mTeSR™1 + 10 μM Y-27632 (STEMCELL Technologies) on day 0. On day1, the differentiation was initiated by replacing the culture medium to 3 mL of STEMdiff™ Mesoderm Induction Medium (STEMCELL Technologies). The same step was repeated on day 2. On day 3, the culture medium was replaced by 4 mL of STEMdiff™ Endothelial Induction Medium (STEMCELL Technologies) to initiate endothelial induction, with the culture medium exchanged on day 5. On day7, we harvest and subculture the hiPSC-derived vascular endothelial cells on 6-well plates coated with animal component-free cell attachment substrate (STEMCELL Technologies), with the culture medium to be STEMdiff™ Endothelial Expansion Medium (STEMCELL Technologies).

Synthesis and characterization of GelMA

GelMA was synthesized following previously established protocols [54] with slight modifications. Briefly, gelatin (300 g Bloom, type A, extracted from porcine skin) was dissolved at 10 wt% in PBS at 50 °C with stirring. Methacrylic anhydride is then added to the 10 wt% gelatin solution dropwise, with a mass ratio of methacrylic anhydride against gelatin to be 0.6:1.0, and react at 50 °C of 2 h. The solution is centrifuged at 3500g for 5 min, and the pH of the collected supernatants is adjusted to 7.4. The solution was then diluted with three parts of deionized water, which was then dialyzed (MWCO 12 kDa, Solarbio) against deionized water at 40 °C for 3 days, with water change 5 times every day, followed by lyophilization for 3 days. The modification degree of the GelMA was characterized with ^{1}H NMR (400 MHz). To quantify the degree of modification of the primary amines, 2,4,6-Trinitrobenzene Sulfonic Acid (TNBS, ThermoFisher Scientific) assay was performed. Briefly, Gelatin or GelMA is dissolved in Sodium Bicarbonate (pH 8.5) at 200 μg mL^{-1}, with the leucine dissolved at 0–30 μg mL^{-1} to serve as the standard curve. For each 0.5 mL of the samples, 0.25 mL 0.1 wt% TNBS was added and reacted for 2 h at 37 °C, followed by adding 0.25 mL 10 wt% Sodium Dodecyl Sulfate (SDS) and 0.125 mL 1 N HCl, and then read the absorbance at 335 nm using a microplate reader (SpectraMax M2, Molecular Devices). The modificaton degree was determined to be 52.0 % (Fig. S1B).

Synthesis and characterization of GelADH and GelADH-FITC

GelADH was synthesized following previously established protocols with slight modifications [13]. Briefly, 1 g of gelatin (300 g Bloom, type A, extracted from porcine skin) was dissolved at 10 wt% in 10 mM pH 5.5 PBS (Biorigin Inc.) at 50 °C with stirring, 1.74 g of adipic dihydrazide (ADH, Aladdin) was added to the solution. Then, 0.77 g of 1-Hydroxybenzotriazole (HOBt, Aladdin) and 0.77 g of N-(3-Dimethylaminopropyl)-N′-ethylcarbodiimide hydrochloride (EDC, Aladdin) were separately dissolved in a 10 mL DMSO/dH2O mixture (1:1), and was added dropwise to the reaction. After adjusting the pH to 5.2, the reaction was maintained at 50 °C with stirring for 12 h. After adjusting the pH to 7.4, the solution was diluted with three parts of deionized water, which was then dialyzed (MWCO 12 kDa, Solarbio) against deionized water at 40 °C for 3 days with 5 times water change every day, followed by lyophilization for 3 days. The GelADH was characterized with ^{1}H NMR (400 MHz), and the modification degree was quantified using the TNBS assay as mentioned above. The modificaton degree was determined to be 29.6 % (Fig. S1B). For the synthesis of GelADH-FITC, 100 mg 5-FITC was dissolved in 2 mL DMSO, which was added to 150 mL of 5 wt% GelADH solution. The pH of the solution was adjusted to 8.1 with 1 N NaOH, and the reaction was maintained at 40 °C with stirring for 3 h. The reaction mixture was diluted with three parts of deionized water and was transferred to dialysis with 5 times water change every day for a week, followed by lyophilization for 3 days.

Synthesis and characterization of DexCHO

DexCHO was synthesized following previously established protocols with slight modifications [13]. Briefly, 1 g of dextran (Mn = 110,000; Sigma- Aldrich) was dissolved at 1 wt% in distilled water, and then 1 g sodium periodate (Aladdin) was added to the solution. The solution was then stirred in the dark for 0.5 h, followed by adding 1.0 mL ethylene glycol to terminate the oxidative reaction and stirring for an additional 0.5 h. The solution was then dialyzed (MWCO 3500, Solarbio) against distilled water for 3 days with water change 5 times every day, followed by lyophilization for 3 days. The DexCHO was characterized with ^{1}H NMR (400 MHz), and the modification degree was quantified by first reacting aldehyde groups to *tert*-Butyl carbazate (t-BC), and then measured the unreacted t-BC concentration by using the TNBS assay [27,55]. In brief, the DexCHO sample was prepared by dissolving DexCHO at 2 wt% (w/v) in distilled water, 0–30 mM of known t-BC standard curve were formulated by dissolving t-BC in 1 wt% trichloroacetic acid. Then, 0.25 mL DexCHO sample was mixed with 0.25 mL 30 mM t-BC solution at room temperature for 24 h. 0.25 mL of the reaction mixture or the t-BC with known concentration was then reacted with 0.5 mL TNBS for 2 h at 37 °C, followed by adding 0.25 mL 10 wt% Sodium Dodecyl Sulfate (SDS) and 0.125 mL 1 N HCL, and then read the absorbance at 335 nm using a microplate reader (SpectraMax M2, Molecular Devices). The modificaton degree was determined to be 19.4 % (Fig. S1C).

Hydrogel formation and stability tests

The hydrogel precursors are dissolved in pH 7.4 PBS (VivaCell) to give stock solutions of 10 wt% GelADH, 10 wt% GelMA containing 0.25 wt% LAP, and 2 wt% DexCHO. GelADH stock solution, either containing GelMA or not, was uniformly mixed with DexCHO stock solution and PBS at certain ratio while avoiding generating bubbles. To assess hydrogel morphology and stability, the hydrogel mixture was then cast in a disposable truncated syringe (1 ml, BD) followed by photo-crosslinking with 405 nm blue light source (EFL) under a light intensity of 30 mW cm^{-2} for 3 min. The formed hydrogel trunks were then gently squeezed out of the syringe onto glass slides or PBS-filled well plates for further observations. To assess GelADH retention and to evaluate storage modulus over incubation or cell culturing, the hydrogel was formed by crosslinking in a PDMS mold with 8 mm diameter and 1 mm thickness.

Rheological test

The mechanical properties of the hydrogels were tested with a Rheometer (MCR 302, Anton Paar) equipped with a 25 mm diameter parallel plate geometry (PP25, Anton Paar). To assess *in situ* hydrogel crosslinking, times sweeps were performed with the photo-rheology plate (P-PTD200/GL, Anton Paar) at 25 °C with 1 Hz frequency, 0.01 % strain, 0.1 mm gap distance, and 80 μL hydrogel sample. 30 mW cm^{-2} UV light (S1500, Omni-Cure) was introduced for the first 3 min if the tested sample have the GelMA hydrogel networks to be photo-crosslinked. For a total measuring duration of 20 min, the storage modulus G' and the loss modulus G'' were monitored. Upon incubation or with cell culturing, the stiffness of the hydrogels was tested by measuring the storage modulus of the hydrogel discs using an 8 mm diameter parallel plate geometry (PP08, Anton Paar) at the desired time point, with 1 Hz frequency and 1 % strain at room temperature. To assess stress relaxation of the hydrogels, 25 mm diameter and 2 mm thickness hydrogel discs were cast in a customized mold, the hydrogel discs were then immersed into PBS for 4 h and were transferred onto the rheometer platform. After a 10 wt% strain was applied over 1 s, a period of 3 h was followed to observe the decay of the relaxation modulus G(t). All the hydrogel samples were sealed with mineral oil at the gap to prevent dehydration. The stress relaxation curves for the GelMA groups are fitted in MATLAB. Briefly, the stress relaxation was fitted into the following generalized Maxwell–Weichert three elements model [23,56]:

$$\sigma = \sigma_0 + \sigma_1 e^{-t/\tau_1} + \sigma_2 e^{-t/\tau_2} \quad (1.1)$$

where σ is the normalized stress. τ_1 and τ_2 are relaxaion time constants that describe the stress decay. The best-fit parameters were obtained using MATLAB (2023a). The decay half-time was then calculated.

3D cell culture with hydrogels

Upon culturing to confluent, the cells were digested and centrifuged (200 g, 3 min). The resulting cell pellet was resuspended in a stock solution of 10 wt% GelADH, with or without 10 wt% GelMA containing 0.25 wt% LAP depending on whether the double network dynamic hydrogel groups were to be formulated. The cell suspension was then uniformly mixed with 2 wt% DexCHO stock solution and PBS in a 0.2 mL PCR microtube to avoid generating bubbles, resulting a HUVECs density of 4×10^6 cells mL^{-1} and the HLFBs density was determined according to the tested HUVEC:HLFB ratio. Each 12.5 uL cell-embedded hydrogel mixture from the total volume was rapidly pipetted into the customized 3D cell culture mold on an ice plate to avoid cell sedimentation. Specifically, the molds were prepared from 24-well round cover slip covered with a layer of adhesive silicon film, that was punctured with holes of 4 mm diameter and 0.8 mm height to be loaded with the hydrogels. Immediately after loading the cell-embedded hydrogels, the molds were transferred onto 405 nm blue light source (EFL) to form the photo-crosslinked GelMA networks under a light intensity of 30 mW cm^{-2} for 2 min. The hydrogels were allowed to react for a further 5 min to ensure sufficient hydrazone bonds formation among the GelADH and the DexCHO macromers. The samples were then immersed with a supplemented EGM2 medium and cultured at 37 °C, with medium change performed every day. The embedding of MSCs and HepG2 spheroids followed the same procefure as described above, with the encapsulated cell density to be 4×10^6 cells mL^{-1} for the MSCs and 3×10^3 spheroids mL^{-1} for the HepG2 spheroids.

GelADH-FITC release test

The GelADH-FITC was used to form the DHs and the DNDHs, followed by incubation or cell culture. The PBS or culture medium supernatant that contained the released GelADH-FITC at the desired time point was collected and measuered with 498 nm activation and 517 nm emission, using the microplate reader (SpectraMax M2, Molecular Devices). The amount of GelADH-FITC released was calculated using a standard reference that is prepared by fully dissolving uncrosslinked GelADH-FITC to PBS or culture medium.

Cytocompatibility test

The cytocompatibility of the double network dynamic hydrogels to HUVECs, and the cytocompatibility of the printed DNDH* to the co-embedded HUVECs and HLFBs, were assessed using the Cell Counting Kit 8 (CCK-8, Dojindo) assay and the alamarBlue™ (ThermoFisher Scientific) assay. After encapsulating the HUVECs with different double network dynamic hydrogel formulations based on the 4 wt% GelMA for 24 h, the culture medium was removed and was replaced by fresh medium supplemented with the CCK-8 or the alamarBlue™ reagent in a ratio to culture medium of 1:10, followed by a 4 h incubation at 37 °C. For the CCK-8 assay, 100 μL of the reacted supernatant from each sample was transferred to a clear-bottom 96-well plate, and the absorbance was measured at 450 nm using a microplate reader (Multiskan FC, ThermoFisher Scientific). For the alamarBlue™ assay, 100 μL of the reacted supernatant from each sample was transferred to a black-bottom 96-well plate, followed by measuring fluorescence with 530 nm activation and 590 nm emission, using the microplate reader (SpectraMax M2, Molecular Devices).

Cellular circularity analysis

The average circularity value is calculated according to the following formula:

$$C = \frac{4\pi A}{P^2} \quad (2.1)$$

where A is the area occupied by the cell and P is the perimeter of the cell, both are derived from image analysis with ImageJ. The representative cell circularity was plotted with MATLAB (2023a).

Immunofluorescence of cell-encapsulated hydrogels

The cell-embedded hydrogel samples are washed with PBS for three times and then fixed with 4 wt% paraformaldehyde (PFA, Solarbio) for 2 h at room temperature, followed by three times wash with PBS. The samples were then blocked with Tris Buffered Saline with Tween® 20 (TBST, Solarbio) that contains 10 wt% goat serum (Solarbio) for 4 h at room temperature. The hydrogel samples were then stained with primary antibodies that were diluted in TBST containing 10 wt% goat serum at 4 °C for 24 h. Primary antibodies of anti CD31 (ab9498, abcam) were used as 1:200 diluted. Anti-Integrin b1 (ab30394, abcam), anti-phospho-FAK (44-624G, ThermoFisher Scientific), anti-MMP14

(ab51074, abcam), anti ColIV (ab86042, abcam) were used as 1:100 diluted. After 6 times wash with TBST, the hydrogel samples were stained with secondary antibodies, Rhodamine labeled Phalloidin (Solarbio) and 4′,6-diamidino-2-phenylindole (DAPI, Solarbio) for 6 h at room temperature. Secondary antibodies of goat anti-mouse 488 (A28175, Invitrogen) or goat anti-rabbit 555 (A21428, Invitrogen) were used at 1:250 dilution. The hydrogel samples were then washed with TBST for 6 times to remove unconjugated antibodies and staining reagents. For observation of the stained hydrogel samples, 100 μm thickness z-stack images were scanned by using a confocal microscope (Dragonfly, Andor). The vascular sprout length and mean tube volume were analyzed in Imaris using the filament tracing tool. The fluorescence intensity was quantified with ImageJ.

Bioink preparation, 3D bioprinting and printability evaluations

The 3D bioprinting process was carried out in a temperature-controlled condition on a bioprinter (Biomaker 2, SunP Biotech) as previously described, with slight modifications [57]. To screen the suitable DNDH formulation that could potentially serve as cell-laden bioinks, a series of DNDHs were prepared using stock solution of GelADH, GelMA, LAP, DexCHO and PBS. Briefly, stock solution of 10 wt% GelADH, and 10 wt% GelMA containing 0.25 wt% LAP was uniformly mixed with 2 wt% DexCHO stock solution and PBS in a 2 mL PCR tube avoid generating bubbles, which was then transffered into 3 mL syringe, stayed for 10 min to allow dynamic crosslinking to occur. In the following printing process, the nozzles were set to be 21 °C and the printing bed was set to be 8 °C. After printing the formulations of the DNDHs into 10 × 10 mm hydrogel grids in 35 mm diameter petri dish, photos of the printed structures were taken and analyzed using the previous methods [31], that utilizes the following formula to assess printability:

$$C = \frac{4\pi A}{L^2} \tag{3.1}$$

$$Pr = \frac{\pi}{4C} = \frac{L^2}{16A} \tag{3.2}$$

The printability (Pr) was determined by comparing the similarity of each individual square window within the filament lattice to a perfect square, from the perimeter (L) and the area (A). For 3D printing in a suspension bath, we take the same printing procedure, except that the priniting take places in a suspension bath of Carbopol gel (*SunP FLOAT II*, SunP Biotech) at room temperature. After suspension printing, the printed structures were obtained and further immersed in PBS for observation the printed geometry. For the 3D printing of cell embeded DNDH bioinks, the cells were harvested by Accutase diggestion and centrifugation, the resulting cell pellet was resuspended in stock solution of 10 wt% GelADH, and 10 wt% GelMA containing 0.25 wt% LAP, 100 ug mL^{-1} laminin and 50 ng mL^{-1} VEGF, which was then uniformly mixed with 2 wt% DexCHO stock solution and PBS in a 2 mL PCR tube avoid generating bubbles, resulting a HUVECs cell density of 4 million mL^{-1} and HUVEC:HLFB ratio of 2:1, the bioink were then transffered into 3 mL syringe, stayed for 10 min to allow dynamic crosslinking to occur, and was printed using the same parameter as printing the DNDHs without embedded cells. After prinitng in 35 mm diameter petri dish, the cell-laden constructs were immersed with 2 mL EGM2 culture medium supplemented with 50 ng mL^{-1} VEGF, and were incubated at 37 °C and 5 % CO_2 for 7 days, with the culture medium changed every two days.

Tubing assay of iPSC-derived ECs

100 μL of growth factor-reduced and phenol red-free Matrigel (356231, Corning) was uniformly pipetted to the bottom of each well of 24 well-plate, followed by incubation at 37 °C for 1 h to allow sufficient gelation. The iPSC-derived ECs were digested and seeded onto Matrigel, in 1 mL of EGM2 per well at a cell density of 5×10^4 cells mL^{-1}. The morphology of the vascular tubes was observed at 12 h by labeling with Calcein-AM (ThermoFisher Scientific).

Animal studies

Sprague-Dawley (SD) rats (4-week-old males; n = 3) were purchased from SPFBiotech. All experiments and procedures were approved by Institutional Animal Care and Use Committee, Sinoresearch (Beijing) Biotechnology Co., Ltd., with the Approval no. ZYZ(202312010). The GelMA and the DNDH* hydrogels were prepared into size of 10 mm diameter and 2 mm height disks, that have supplemented with 100 μg mL^{-1} laminin. 50 ng mL^{-1} VEGF is supplemented to the hydrogel groups upon the condition The animals were anesthetized and the hydrogels were then transplanted into the subcutaneous region of the SD rats. After a week, the animals were euthanized, and the hydrogels were harvested. The samples were fixed in 4 wt % Paraformaldehyde (PFA, Solarbio), which were then excised and prepared for H&E, Masson and immunohistochemistry staining. To visualize the angiogenesis of the transplanted hydrogel, the rats were injected with Dextran-FITC (2,000 KDa) via the tail vein at a concentration of 1 mg mL^{-1}. After 30 min of circulation, the animals were euthanized, and the hydrogels were harvested and directly observed under a confocal microscope.

Statistical analysis

All statistical analyses were performed using *GraphPad Prism 8.0.2*. Unless otherwise noted, all data are presented as mean ± standard deviation. All statistical significance was analyzed by a two-tailed unpaired Student's *t* test.

Data availability

All data needed to evaluate the conclusions in the paper are present in the paper and/or the Supplementary Materials.

CRediT authorship contribution statement

Runze Xu: Writing – original draft, Visualization, Methodology, Investigation, Conceptualization. **Bohan Dou:** Methodology, Formal analysis, Data curation. **Shuang Yu:** Methodology, Formal analysis, Data curation. **Ziyu Wang:** Methodology. **Yanli Zhang:** Methodology, Data curation. **Ling Leng:** Methodology, Formal analysis, Data curation. **Liliang Ouyang:** Writing – review & editing, Visualization, Supervision, Project administration, Funding acquisition, Conceptualization. **Wei Sun:** Writing – review & editing, Supervision, Project administration, Conceptualization.

Data availability

Data will be made available on request.

Declaration of competing interest

The authors declare the following financial interests/personal relationships which may be considered as potential competing interests: W. Sun, L. Ouyang and R. Xu have applied for a Chinese Patent related to this study (file No. 2023080479). Other authors declare no conflict of interest.

Acknowledgments

The authors acknowledge the financial support from the National Natural Science Foundation of China (No. 52105306, No. 32211530075, No. 52475305), the "111" Plan Project (No. B17026). The authors acknowledge Dr. Tiankun Liu for kindly providing the HLFBs and help with cell culture, and Honson Ooi for help with manuscript proofreading. L.O. acknowledges the general support from Dr. Z. Xiong, Dr. F. Lin, Dr. T. Zhang, and Dr. L. Zhang.

Appendix A. Supplementary material

Supplementary data to this article can be found online at https://doi.org/10.1016/j.mattod.2025.01.019.

References

[1] D.Z. Zhou et al., Inter. J. Extr. Manufact. 5 (2023) .
[2] M. Potente, T. Maekinen, Nat. Rev. Mol. Cell Biol. 18 (2017) 477–494.
[3] Z. Wei et al., Adv. Drug Deliv. Rev. 149 (2019) 95–106.
[4] K.M. Park, S. Gerecht, Development 141 (2014) 2760–2769.
[5] G.D. Yancopoulos et al., Nature 407 (2000) 242–248.
[6] Y. Guan, L. Racioppi, S. Gerecht, Nat. Rev. Mater. 8 (2023) 688–699.
[7] Z.Q. Fu et al., Mater. Today 52 (2022) 112–132.
[8] M. Campisi et al., Biomaterials 180 (2018) 117–129.
[9] D. Rutsche et al., Adv. Mater. 35 (2023) .
[10] Y.C. Chen et al., Adv. Funct. Mater. 22 (2012) 2027–2039.
[11] B.G. Soliman et al., Adv. Healthc. Mater. 11 (2022) .
[12] L.L. Ouyang, Trends Biotechnol. 40 (2022) 891–902.
[13] Z. Wei et al., Cell Stem Cell 27 (2020) . 798-+.
[14] D.D. McKinnon et al., Adv. Mater. 26 (2014) 865–872.
[15] A.R. Cameron, J.E. Frith, J.J. Cooper-White, Biomaterials 32 (2011) 5979–5993.
[16] A.R. Cameron et al., Biomaterials 35 (2014) 1857–1868.
[17] F.L.C. Morgan, L. Moroni, M.B. Baker, Adv. Healthc. Mater. 9 (2020) .
[18] H.D. Lu et al., Adv. Healthc. Mater. 2 (2013) 1028–1036.
[19] L.L. Wang et al., J. Biomed. Mater. Res. A 106 (2018) 865–875.
[20] L. Trachsel et al., Biomacromolecules 20 (2019) 4502–4511.
[21] T. Li et al., Acta Biomater. 156 (2023) 21–36.
[22] C. Loebel, R.L. Mauck, J.A. Burdick, Nat. Mater. 18 (2019) . 883-+.
[23] A. Chrisnandy et al., Nat. Mater. 21 (2022) . 479-+.
[24] K.H. Vining et al., Nat. Mater. 21 (2022) . 939-+.
[25] M.X. Zhu et al., Sci. Rep. 9 (2019) .
[26] R.B. Freedman, G.K. Radda, Biochem. J. 108 (1968) 383–1000.
[27] A.N. Borelli et al., Adv. Healthc. Mater. 11 (2022) .
[28] H.P. Lee et al., Nat. Mater. 16 (2017) 1243-+.
[29] J. He et al., Adv. Healthc. Mater. 12 (2023) .
[30] L.L. Ouyang et al., Sci. Adv. 6 (2020) .
[31] L.L. Ouyang et al., Biofabrication 8 (2016) .
[32] N. Huebsch et al., Nat. Mater. 9 (2010) 518–526.
[33] B.G. Yang et al., Nat. Commun. 12 (2021) .
[34] J.Z. Kechagia, J. Ivaska, P. Roca-Cusachs, Nat. Rev. Mol. Cell Biol. 20 (2019) 457–473.
[35] H.H.G. Song et al., Adv. Funct. Mater. 30 (2020) .
[36] V.V. Orlova et al., Nat. Protoc. 9 (2014) 1514–1531.
[37] R.S. Apte, D.S. Chen, N. Ferrara, Cell 176 (2019) 1248–1264.
[38] J. Gautam, X.M. Zhang, Y. Yao, Sci. Rep. 6 (2016) .
[39] A.E.G. Baker et al., Adv. Mater. 31 (2019) .
[40] J. Ishihara et al., Nat. Commun. 9 (2018) .
[41] K. Stamati et al., Exp. Cell Res. 327 (2014) 68–77.
[42] O. Dobre et al., Adv. Funct. Mater. 31 (2021) .
[43] D.G. Belair et al., Stem Cell Rev. Rep. 11 (2015) 511–525.
[44] S. Kusuma et al., PNAS 110 (2013) 12601–12606.
[45] R.A. Wimmer et al., Nature 565 (2019) . 505-+.
[46] B. Trappmann et al., Nat. Commun. 8 (2017) .
[47] T. Feijao et al., Biomaterials 279 (2021) .
[48] O.A. Peña, P. Martin, Nat. Rev. Mol. Cell Biol. 25 (2024) 599–616.
[49] S. Butenko et al., Nat. Commun. 15 (2024) .
[50] S. Nam et al., Biomaterials 200 (2019) 15–24.
[51] Z. Wei et al., Nat. Commun. 14 (2023) .
[52] M. Diba et al., Adv. Mater. 33 (2021) .
[53] D.H. Kang et al., Cell Rep. 42 (2023) .
[54] D. Loessner et al., Nat. Protoc. 11 (2016) 727–746.
[55] W.Y. Su, Y.C. Chen, F.H. Lin, Acta Biomater. 6 (2010) 3044–3055.
[56] B. Babaei et al., J. Mech. Behav. Biomed. Mater. 55 (2016) 32–41.
[57] Y. Yang et al., Inter. J. Bioprint. 8 (2022) 145–160.